

1 **Neuroimaging-AI Endophenotypes of Brain Diseases in the General** 2 **Population: Towards a Dimensional System of Vulnerability**

3
4 Junhao Wen^{1*}, Ioanna Skampardoni², Ye Ella Tian³, Zhijian Yang², Yuhan Cui², Guray Erus²,
5 Gyujoon Hwang², Erdem Varol⁴, Aleix Boquet-Pujadas⁵, Ganesh B. Chand⁶, Ilya Nasrallah²,
6 Theodore Satterthwaite⁷, Haochang Shou², Li Shen⁸, Arthur W. Toga⁹, Andrew Zalesky³,
7 Christos Davatzikos^{2,*}

8
9 ¹Laboratory of AI and Biomedical Science (LABS), Stevens Neuroimaging and Informatics Institute, Keck School
10 of Medicine of USC, University of Southern California, Los Angeles, California, USA

11 ²Artificial Intelligence in Biomedical Imaging Laboratory (AIBIL), Center for AI and Data Science for Integrated
12 Diagnostics (AI²D), Perelman School of Medicine, University of Pennsylvania, Philadelphia, USA

13 ³Melbourne Neuropsychiatry Centre, Department of Psychiatry, Melbourne Medical School, The University of
14 Melbourne, Melbourne, Victoria, Australia

15 ⁴Department of Computer Science and Engineering, New York University, New York, USA

16 ⁵Biomedical Imaging Group, EPFL, Lausanne, Switzerland

17 ⁶Department of Radiology, School of Medicine, Washington University in St. Louis, St. Louis, MO, USA

18 ⁷Department of Psychiatry, Perelman School of Medicine, University of Pennsylvania, Philadelphia, USA

19 ⁸Department of Biostatistics, Epidemiology and Informatics University of Pennsylvania Perelman School of Medicine,
20 Philadelphia, USA

21 ⁹Laboratory of Neuro Imaging (LONI), Stevens Neuroimaging and Informatics Institute, Keck School of Medicine
22 of USC, University of Southern California, Los Angeles, California, USA

23
24 *Corresponding authors:

25 Junhao Wen, junhaowe@usc.edu

26 2025 Zonal Ave, Los Angeles, CA 90033, United States

27 Christos Davatzikos, christos.davatzikos@penntoolbox.upenn.edu

28 3700 Hamilton Walk, 7th Floor, Philadelphia, PA 19104, United States

29
30 Word counts: 5669 words

31 Abstract

32 Disease heterogeneity poses a significant challenge for precision diagnostics in both clinical and
33 sub-clinical stages. Recent work leveraging artificial intelligence (AI) has offered promise to
34 dissect this heterogeneity by identifying complex intermediate phenotypes – herein called
35 dimensional neuroimaging endophenotypes (DNEs) – which subtype various neurologic and
36 neuropsychiatric diseases. We investigate the presence of nine such DNEs derived from
37 independent yet harmonized studies on Alzheimer's disease (AD1-2)¹, autism spectrum disorder
38 (ASD1-3)², late-life depression (LLD1-2)³, and schizophrenia (SCZ1-2)⁴, in the general
39 population of 39,178 participants in the UK Biobank study. Phenome-wide associations revealed
40 prominent associations between the nine DNEs and phenotypes related to the brain and other
41 human organ systems. This phenotypic landscape aligns with the SNP-phenotype genome-wide
42 associations, revealing 31 genomic loci associated with the nine DNEs (Bonferroni corrected P-
43 value $< 5 \times 10^{-8}/9$). The DNEs exhibited significant genetic correlations, colocalization, and causal
44 relationships with multiple human organ systems and chronic diseases. A causal effect (odds
45 ratio=1.25 [1.11, 1.40], P-value= 8.72×10^{-4}) was established from AD2, characterized by focal
46 medial temporal lobe atrophy, to AD. The nine DNEs and their polygenic risk scores
47 significantly improved the prediction accuracy for 14 systemic disease categories and mortality.
48 These findings underscore the potential of the nine DNEs to identify individuals at a high risk of
49 developing the four brain diseases during preclinical stages for precision diagnostics. All results
50 are publicly available at: <http://labs.loni.usc.edu/medicine/>.

51 Main

52 Disease heterogeneity^{2,3,5-10} has been a significant challenge for precision medicine¹¹, including
53 precision neuroscience. A new era powered by artificial intelligence (AI) and large-scale, multi-
54 omics biomarkers may enable us to quantify individualized liability for various brain
55 diseases^{12,13}. Recent work has leveraged semi-supervised clustering methods (**Fig. 1a** and
56 **Supplementary eMethod 1**) to tackle this challenge. These methods characterize the disease
57 heterogeneity by constructing a mapping or transformation from a reference group (e.g., healthy
58 controls) to a target group (i.e., patients with a specific disease). In clinical neuroscience, these
59 methods can quantify deviation from typical brain structure measured by T1-weighted magnetic
60 resonance imaging (MRI)¹⁻⁴. They represent disease-related neuroanatomical heterogeneity via k
61 low-dimensional categorical subtypes associated with specific patterns of brain change relative
62 to the reference group. Instead of focusing on the k categorical subtypes, we investigated their
63 corresponding continuous phenotypes¹⁴, given that brain diseases develop along a continuous
64 spectrum. Each neuroanatomical pattern's level of expression, therefore, serves as a dimensional
65 AI-derived biomarker pertinent to the respective disease.

66 Previous heterogeneity research has primarily focused on within-disease
67 heterogeneity^{2,3,5-10}. However, this approach neglects the shared etiology, genetics, and clinical
68 manifestations among different brain diseases. Conversely, while several studies have
69 investigated the shared genetic components across various brain diseases, they have overlooked
70 the important aspect of disease heterogeneity within each condition^{15,16}. As such, a broad
71 perspective is required to simultaneously investigate disease heterogeneity, spanning multiple
72 neurodegenerative and neuropsychiatric disorders. This holistic approach aids in understanding
73 the commonalities and interrelationships between these brain diseases and multi-organ systems
74 of the human^{17,18}. Such an effort could simultaneously capture neurobiological heterogeneity
75 within disorders and explain shared features, mechanisms, and risk factors across disorders.
76 Ultimately, unraveling neurobiological heterogeneity within neuropsychiatric syndromes and
77 explaining co-morbidity among them promises to accelerate more effective diagnosis, treatment,
78 and prevention strategies.

79 Recent work leveraging AI-derived biomarkers identified using semi-supervised learning
80 has offered novel ways to capture complex neuroanatomical heterogeneity within disease
81 populations^{2,3,5-9}. However, whether these biomarkers are present in the general population,
82 potentially simultaneously, remains unknown. Here, we sought to measure the presence of
83 multiple AI-based signatures in the general population, delineate common mechanisms among
84 them, and shed light on their relationship with numerous human organ systems^{17,18}. To do this,
85 we capitalized on nine imaging biomarkers recently derived from regional gray matter (GM)
86 volumetrics derived from several large-scale disease-focused consortia, including ADNI¹⁹ for
87 Alzheimer's disease (AD1-2), ABIDE²⁰ for autism spectrum disorder (ASD1-3), LLD³ for late-
88 life depression older than 65 years old (LLD1-2), and PHENOM⁴ for schizophrenia (SCZ1-2).
89 We first conceptualized these biomarkers as the dimensional neuroimaging endophenotype
90 (DNE), seeking to test the endophenotype hypothesis in psychiatry²¹⁻²³, which suggests that such
91 measurable intermediate biomarkers (i.e., the endophenotypes) serve as intermediate phenotypes
92 between genetics and clinical symptoms of the disease. They are thought to be more closely
93 related to the underlying etiology (or genetics) than the complex clinical symptoms or the disease
94 itself.

95 In this study, we evaluated the manifestation of the nine DNEs in the general population
96 using the extensive and comprehensive multi-omics data available in the UK Biobank study²⁴

97 (UKBB, **Method 1**), collected from more than 500,000 participants in the United Kingdom. The
98 pre-trained AI models (**Method 2**) from the four disease populations were applied to the 39,178
99 participants with brain MRI²⁵ and genetic²⁶ data from the UKBB general population. To
100 delineate the phenotypic landscape of the nine DNEs, we first tested whether the
101 neuroanatomical patterns of the nine DNEs are present in the UKBB general population.
102 Subsequently, we conducted a phenome-wide association study (PWAS, **Method 3**) to establish
103 associations between the nine DNEs and additional 611 UKBB phenotypes, including brain
104 imaging-derived phenotypes (IDPs), traits related to multiple human organ systems, cognition,
105 and lifestyle factors. To depict their genetic architecture, we performed a genome-wide
106 association study (GWAS, **Method 4**) linking the nine DNEs to 6,477,810 quality-checked
107 common single nucleotide polymorphisms (SNPs). Furthermore, we conducted analyses to
108 investigate genetic correlations, colocalization, and causal relationships between the nine DNEs,
109 nine human organ systems, and several chronic diseases. Finally, we assessed the ability of the
110 nine DNEs and their corresponding PRSs to predict 14 systemic disease categories and mortality
111 (**Method 5**).

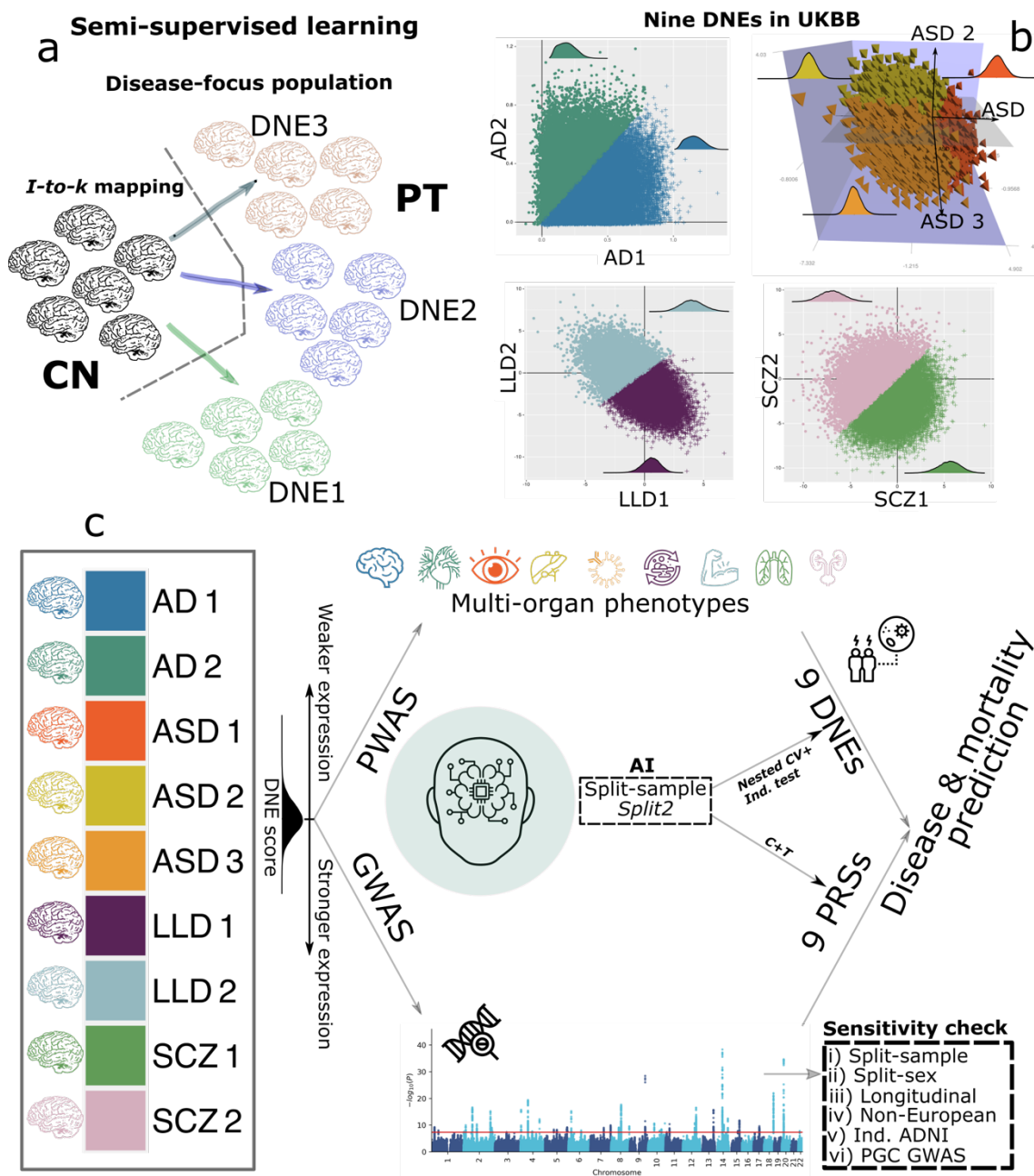
112

113 **Results**

114 Our analytic framework involves computational genomics, statistical methods, and machine
115 learning to elucidate the phenotypic landscape and genetic architecture of the nine DNEs, as
116 illustrated in **Fig. 1**.

117

118 **Figure 1: Study workflow**



119
 120 **a)** The concept of semi-supervised learning methods used in this study (**Method 1**). These AI
 121 methods model the patterns and transformations from the healthy control (CN) to the patient
 122 (PT) domain, thus capturing variations related to underlying disease pathology. Nine DNEs
 123 previously published¹⁻⁴ from four disease-focused, case-control studies were investigated,
 124 including ADNI¹⁹ for Alzheimer's disease (AD1-2), ABIDE²⁰ for autism spectrum disorder
 125 (ASD1-3), LLD³ for late-life depression older than 65 years old (LLD1-2), and PHENOM⁴ for
 126 schizophrenia (SCZ1-2). **b)** The expression of the nine DNEs in the UK Biobank (UKBB)
 127 general population. The trained models were then applied to the UKBB population to quantify
 128 the expression of the neuroanatomical patterns of the nine DNEs at individual levels; a higher

129 DNE score indicates a greater expression (manifestation/presence) of the respective
130 neuroanatomical pattern. For example, the blue samples express predominantly AD2, whereas
131 the pink sample express predominantly SCZ2. The kernel density estimate for each DNE is
132 shown. **c)** Phenome- and genome-wide analyses performed in this study for the nine DNEs.
133 phenome-wide association studies (PWAS) were conducted to associate the nine DNEs with
134 phenotypes across nine organ systems, cognition, and lifestyle factors. Genome-wide association
135 studies (GWAS) were performed to investigate associations between the nine DNEs and
136 common genetic variants (SNPs). Finally, the nine DNEs and their polygenic risk scores
137 predicted 14 disease categories (ICD-10-based) and mortality.

138

139 **All nine DNEs are evident in the general population**

140 We tested whether the neuroanatomical patterns defined in the four disease populations could be
141 found in the general population. We applied the DNE models pre-trained for each disease
142 population to the UKBB general population to measure the degree of expression of each DNE at
143 the individual level.

144 We first summarize the neuroanatomical patterns of the nine DNEs (**Fig. 2a** and **Method**
145 **3b**). The original patterns identified in the disease populations¹⁻⁴ manifest in the general
146 population. AD1 exhibits a pattern of brain atrophy (i.e., negative correlation) across various
147 brain volumes, while AD2 involves focal atrophy of the medial temporal lobe and hippocampus.
148 ASD1 captures a pattern of mildly lower GM volumes in several subcortical regions, including
149 the pallidum, amygdala, and putamen, whereas ASD2 reflects a pattern of relatively larger GM
150 volumes (i.e., positive correlation) in subcortical regions. ASD3, conversely, is characterized by
151 relatively larger GM volumes in several cortical areas, including the insula. LLD1 (positive
152 correlation) and LLD2 (negative correlation) are characterized by widespread patterns of
153 regional GM volumes, including the middle frontal gyrus, the insula, and the thalamus. For
154 schizophrenia, a widespread pattern of reduced brain volumes (e.g., insula) is associated with
155 SCZ1, whereas SCZ2 displays increased volumes of the putamen and pallidum. The details of
156 the P-value, sample sizes, and β values of the linear regression are presented in **Supplementary**
157 **eFile 1** (from disease-specific populations¹⁻⁴) and **2** (from UKBB).

158 Compared to the disease populations, the neuroanatomical patterns of the nine DNEs
159 displayed remarkable deviations in the general population. These deviations were characterized
160 by significant over- and under-expression, except for ASD2, after correcting for multiple
161 comparisons using the Bonferroni method (**Fig. 2b**). For instance, AD1, characterized by diffuse
162 brain atrophy in the ADNI data, showed a significant under-expression (i.e., a smaller mean of
163 the DNE score) in the general population. Conversely, the subcortical atrophy pattern originally
164 identified in ASD1 from the ABIDE data displayed a significant over-expression (i.e., a larger
165 mean of the DNE score) in the participants from the general population.

166 These results provided compelling evidence that the nine DNEs are present in the general
167 population. The contrast in their expression (i.e., over- and under-expression) between the
168 disease-specific and UKBB general populations is expected and underscores their potential
169 relevance as sub-clinical or vulnerability quantitative indices.

170

171 **The nine DNEs exhibit phenotypic associations with traits beyond the brain**

172 To delineate their phenotypic landscape, we associated the nine DNEs with 611 phenotypes in
173 UKBB. To avoid circularity, the PWAS did not include the 119 GM ROIs derived from T1-

174 weighted MRI, from which the nine DNEs were derived. Out of the 611 additional clinical traits
175 spanning multiple organ systems, cognition, and lifestyle factors, we discovered 1818 significant
176 associations after applying the Bonferroni correction (P-value < 0.5/611) (**Fig. 2c**,
177 **Supplementary eFile 2**, and **Method 3c**).

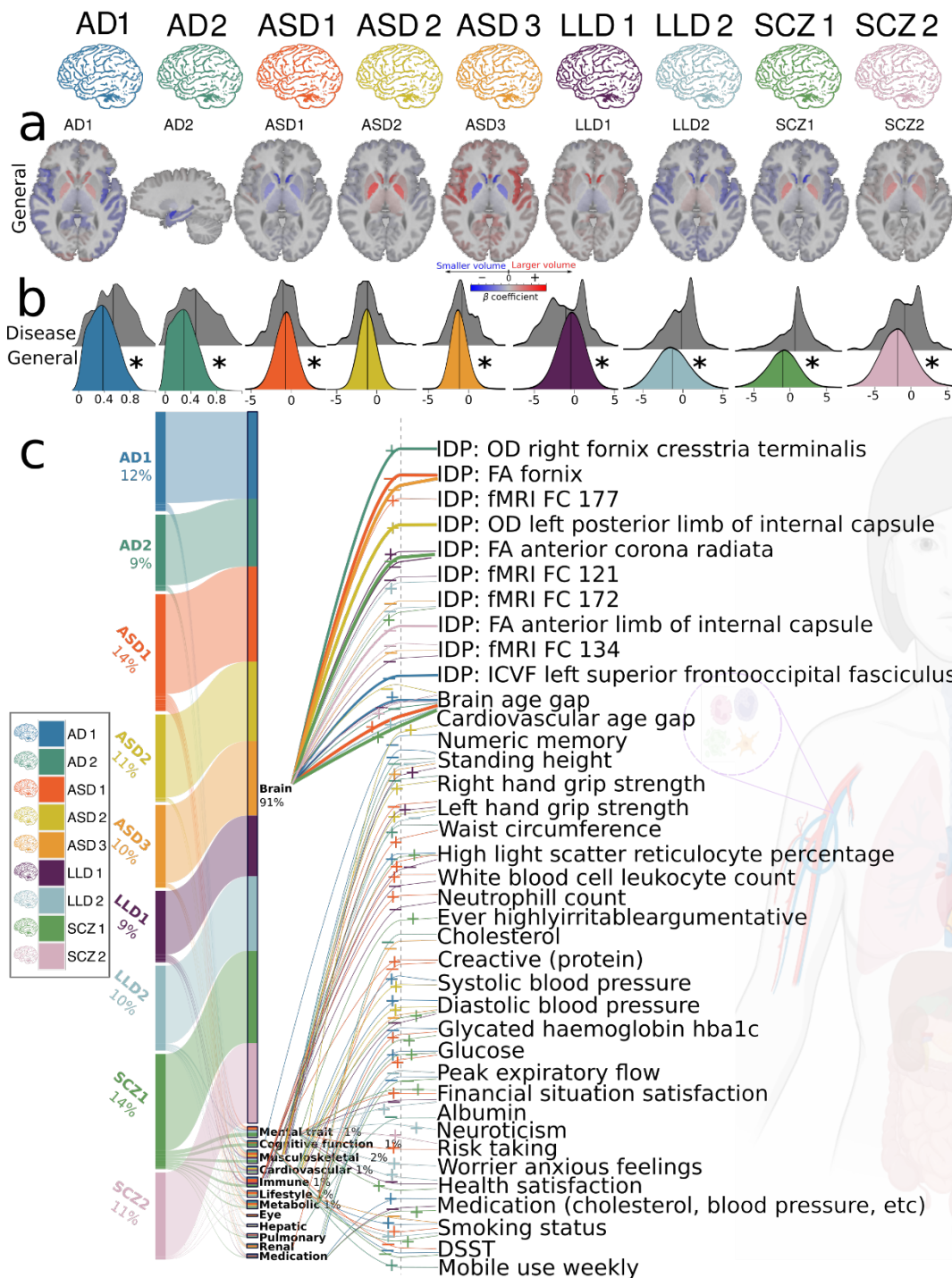
178 Of the 1818 significant associations, 91% were related to the brain. For example, the
179 mean intracellular volume fraction in the superior frontal-occipital fasciculus derived from the
180 multi-shell NODDI²⁸ model was significantly associated with AD1 [$\beta=-0.67\pm0.02$, $-\log_{10}(\text{P-}$
181 $\text{value}) > 300$]. Multiple DNEs were significantly associated with the biological age gap (BAG:
182 AI-predicted age minus chronological age) of the brain [e.g., SCZ2: $\beta=0.19\pm0.01$, $-\log_{10}(\text{P-}$
183 $\text{value})=50.10$]. Furthermore, 2% of the phenotypes related to the musculoskeletal system were
184 associated with the nine DNEs. The nine DNEs were also largely associated with many
185 phenotypes related to mental health (1%). For example, the neuroticism score was significantly
186 associated with LLD2 [$\beta=-1.09\times10^{-2}\pm2.42\times10^{-3}$, $-\log_{10}(\text{P-value})=5.20$] (**Supplementary eFile 3**).

187 We conducted two sensitivity analyses to validate the main PWAS results (**Method 3c**).
188 We obtained high concordance rates in split-sample (98.03%) and sex-stratified analyses
189 (93.98%). Detailed results can be found in **Supplementary eText 1** and **Supplementary eFile 4**
190 and **5** for split-sample and sex-stratified analyses.

191 As anticipated, 91% of the significant associations were linked to the brain, given that the
192 DNEs were derived from regional brain volumetrics in brain disease-specific populations.
193 However, it is noteworthy that these phenotypic associations extended beyond the brain,
194 providing evidence for the significant associations between the brain and the rest of the body.

195
196

Figure 2: Phenome-wide associations of the nine DNEs



197
198 **a)** The neuroanatomical patterns of the nine DNEs were manifested in the UKBB general
199 population and were concordant with the patterns initially derived from the original disease
200 populations¹⁻⁴. A linear regression model was applied to the 119 gray matter regions of interest
201 (ROIs) derived from T1-weighted MRI data while accounting for various covariates (**Method**
202 **3b**). We present the β coefficients of the ROIs that withstood the Bonferroni correction. Positive

203 correlations are depicted using warm reddish colors, while cold blue colors represent negative
204 correlations. For AD2, we showed the sagittal view to visualize the hippocampus and medial
205 temporal lobe. **b)** The nine DNEs are over-expressed (i.e., a higher mean of the DNE score in the
206 population) and under-expressed (i.e., a lower mean of the DNE score) in the general population
207 compared to the disease populations. The kernel density estimates of the nine DNEs are shown
208 for both the training dataset (gray-colored in patients) and the independent test dataset from the
209 UK Biobank (UKBB). Significant differences that survived the Bonferroni corrections between
210 the training and independent test datasets (two-sampled t-test) are denoted with the symbol *. **c)**
211 Phenome-wide associations (PWA) between the nine DNEs (left panel) and 611 phenotypes
212 (middle panel) are dominated by brain phenotypic measures. The length of each rectangle block
213 indicates the percentage of associations for each DNE or phenotype category. The right panel
214 shows representative phenotypes linked to multiple phenotype categories with the highest
215 statistical significance after the Bonferroni correction ($P\text{-value} < 0.05/611$). A thicker colored line
216 corresponds to a higher value of $-\log_{10}(P\text{-value})$. The symbols "+" and "-" represent positive and
217 negative correlations.

218

219 **Genome-wide associations identify 66 genomic loci associated with the nine DNEs**

220 At the genome-wide significance level ($P\text{-value} < 5 \times 10^{-8}$), GWAS (**Method 4a**) identified 10, 8,
221 5, 21, 9, 1, 3, 3, and 6 genomic loci significantly associated with AD1, AD2, ASD1, ASD2,
222 ASD3, LLD1, LLD2, SCZ1, and SCZ2, respectively (66 in total, **Fig. 3a**, and **Supplementary**
223 **eFile 6**). At a more stringent significance level ($P\text{-value} < 5 \times 10^{-8}/9$), 31 loci passed the Bonferroni
224 correction. Notably, 41 loci are novel – their top lead SNP was not associated with any clinical
225 traits in the EMBL-EBI GWAS Catalog²⁹, as annotated in **Fig. 3a** (**Method 4c**, query date: 2nd
226 June 2023, via FUMA version: v1.5.4). To support the robustness of our GWAS, we estimated
227 the intercept of linkage disequilibrium score regression (LDSC)³⁰ and obtained intercepts of
228 1.003, 1.0314, 0.9969, 1.0155, 1.0129, 1.0131, 1.0166, 1.0109, 1.0127 for the nine DNEs. All
229 intercepts were close to 1, indicating no substantial genomic inflation in our GWASs. The
230 Manhattan and QQ plots of the nine GWASs are presented in **Supplementary eFigure 2-10**.

231 All DNEs are significantly heritable ($0.24 < h^2 < 0.66$, $P\text{-value} < 1 \times 10^{-10}$) after Bonferroni
232 correction (**Fig. 3a**, **Supplementary eTable 1**, and **Method 4b**). We employed the GCTA³¹
233 software to estimate h^2 , acknowledging that previous research^{32,33} has demonstrated variations in
234 the magnitude of h^2 estimates based on the choice of methods.

235 We further investigated the significant genomic loci by mapping them to protein-
236 encoding genes and examining their functional implications through expression quantitative trait
237 loci (eQTL) mapping. **Supplementary eFigure 1** presents the regional Manhattan plot for the
238 most significant genomic locus associated with each DNE. For example, we identified a locus
239 associated with ASD2 (top lead SNP: rs3068507 at 20q11.21) and a neighboring locus associated
240 with SCZ1 (top lead SNP: rs6088962 at 20q11.21), both of which mapped to the *MYLK2* gene
241 (**Supplementary eFigure 1d** and **h**). *MYLK2* encodes a myosin light chain kinase primarily
242 expressed in adult skeletal muscle.

243 We conducted six sensitivity analyses to validate the main GWAS results (**Method 4a**).
244 Overall, we obtained high concordance rates in split-sample, sex-stratified (63.26-92.54%), and
245 longitudinal GWAS analyses (100%, $N=1116$), but the concordance rates were relatively low in
246 non-European ancestry GWAS, independent ADNI GWAS, and six case-control GWAS³⁴⁻³⁹ of
247 neurodegenerative and neuropsychiatric disorders from the psychiatric genetic consortium. Refer
248 to **Supplementary eText 2** and **Supplementary eTable 2** for details. The sample sizes for the

249 non-European ($N=4783$) and ADNI ($N=1555$) samples are small; the case-control GWAS from
250 the psychiatric genetic consortium may overlook the heterogeneity within each disease. Detailed
251 results are presented in **Supplementary eText 2** for the sensitivity results, **Supplementary eFile**
252 **7-12** for replicated SNPs/loci, and **Supplementary eFigures 2-10** for Manhattan and QQ plots
253 and the LDSC intercepts. In addition, all GWAS results are also publicly available in the
254 MEDICINE web portal: <http://labs.loni.usc.edu/medicine/>. In conclusion, our GWASs identified
255 many novel genomic loci that previous case-control GWASs might have missed.

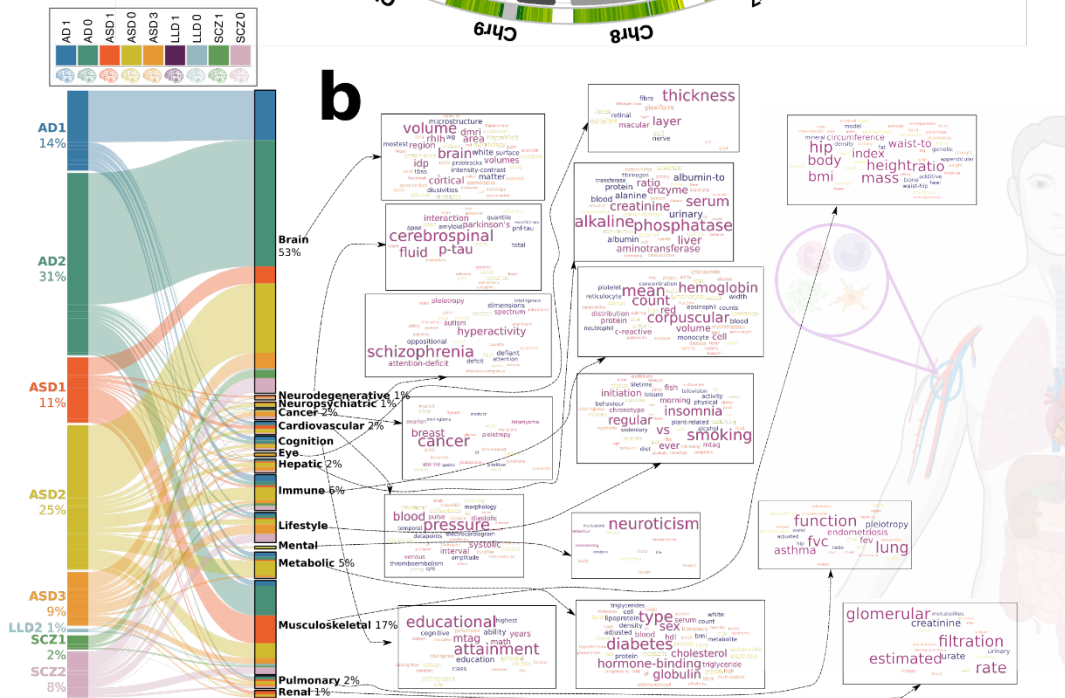
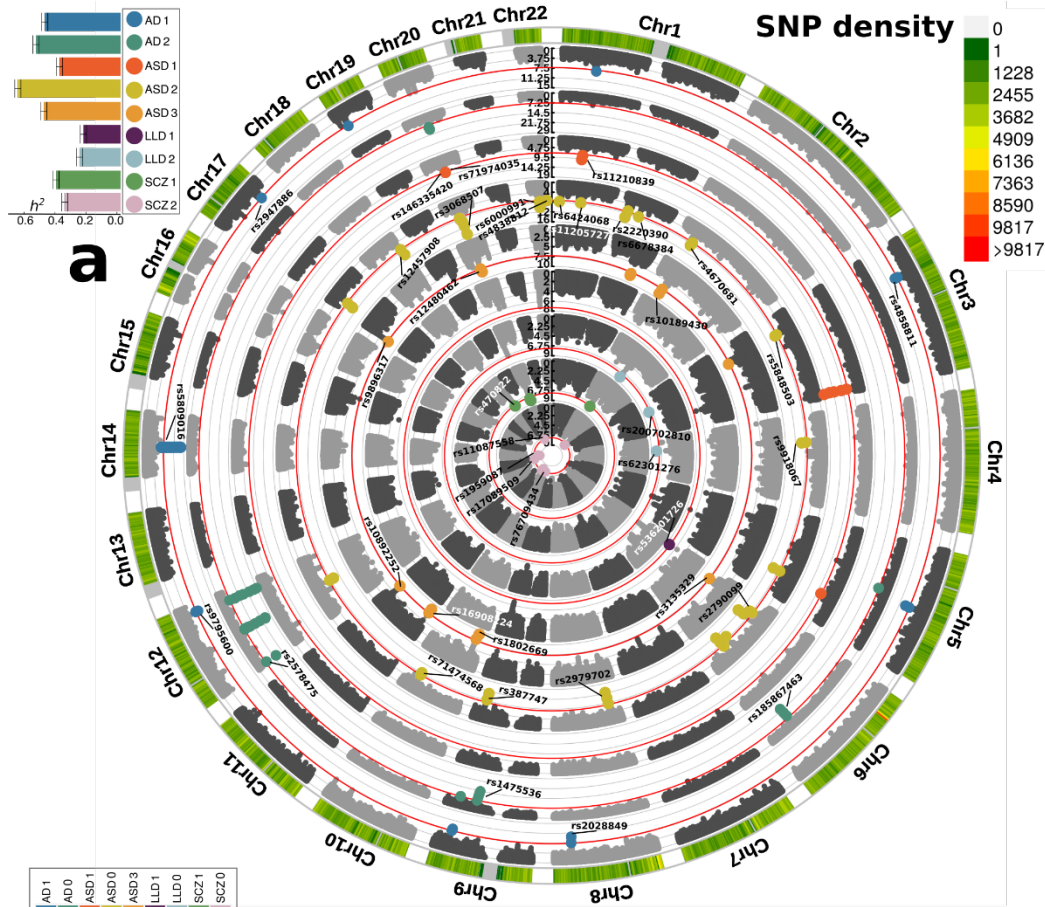
256 **The genetic associations of the nine DNEs parallel their phenotypic associations**

258 We performed a phenome-wide look-up analysis (**Method 4d**) to understand the phenotypic
259 associations of these identified genomic loci in the literature.

260 In total, 2525 clinical traits were associated with genetic variants in our GWAS,
261 including traits linked to multiple organ systems, cognition, and lifestyle factors (**Fig. 3b** and
262 **Supplementary eFile 13**). The genomic loci were largely associated with clinical traits of the
263 brain (53%), musculoskeletal (17%), immune system (6%), neurodegenerative (1%), and
264 neuropsychiatric (1%) diseases. For example, AD2 genomic loci were largely associated with
265 traits related to the brain (565 out of 781, e.g., IDPs), musculoskeletal (133/781, e.g., standing
266 height), immune (17/781, e.g., reticulocyte count), cognition (15/781, e.g., cognitive
267 performance), lifestyle factors (13/781, e.g., smoking), and neurodegenerative traits (1/781, i.e.,
268 neurofibrillary tangles).

269 The findings closely align with the phenotypic associations observed in **Fig. 2c**,
270 reinforcing that the DNEs share genetic determinants linked to organs beyond the brain, lifestyle
271 factors, and cognition.

272 **Figure 3: Genome-wide associations of the nine DNEs**



273
 274 **a)** Genome-wide associations identified 66 (10, 8, 5, 21, 9, 1, 3, 3, 6 for the nine DNEs) genomic
 275 loci ($P\text{-value} < 5 \times 10^{-8}$) associated with the nine DNEs. Using the top lead SNP, we denoted the 41
 276 novel genomic loci – not associated with any clinical traits in the EMBL-EBI GWAS Catalog.

277 The left legend indicates the significant SNP-based heritability (h^2) for the nine DNEs; the right
278 legend represents the SNP density of our genetic data throughout the human genome. GWAS
279 was performed using the Genome Reference Consortium Human Build 37 (GRCh37). **b)**
280 Phenome-wide association query of the previously identified genomic loci (left panel) in the
281 EMBL-EBI GWAS Catalog (via FUMA 1.4.2) shows a brain-dominant genetic architecture. We
282 categorized all clinical traits (middle panel) into several high-level categories linked to multiple
283 organ systems, neurodegenerative and neuropsychiatric disorders, lifestyle factors, etc. We then
284 show the keyword cloud plots for each category (right panel).

285

286 **The genetic correlation of the nine DNEs**

287 To understand the shared genetic underpinnings, we estimated the genetic correlation³⁰ (g_c)
288 (**Method 4e**) between the nine DNEs, the BAG of nine human organ systems, and six brain
289 diseases (AD, attention-deficit/hyperactivity disorder, autism spectrum disorder, bipolar,
290 obsessive-compulsive disorder, schizophrenia; **Supplementary eTable 2**) from the psychiatric
291 genetic consortium.

292 We first estimated the g_c between each pair of DNEs (**Fig. 4a**). Numerous DNEs
293 exhibited strong genetic correlations with each other. Among these, the highest positive genetic
294 correlation was obtained between ASD2 and SCZ1 ($g_c=0.57\pm 0.04$); the highest negative genetic
295 correlations were obtained between ASD2 and ASD1 ($g_c=-0.55\pm 0.04$), and between ASD3 and
296 SCZ1 ($g_c=-0.51\pm 0.05$). We also observed a substantial alignment between the phenotypic
297 correlation (p_c) and the genetic correlation of pairwise DNEs, supporting the long-standing
298 Cheverud's Conjecture⁴⁰. However, we identified two exceptions where the observed phenotypic
299 and genetic correlations exhibited opposite directions. ASD1 and ASD3 showed a negative
300 phenotypic ($p_c=-0.39\pm 0.08$) but a positive genetic correlation ($g_c=0.21\pm 0.05$); ASD1 and LLD1
301 showed a negative phenotypic ($p_c=-0.34\pm 0.09$) but a positive genetic correlation ($g_c=0.16\pm 0.07$)
302 (**Supplementary eTable 3**). This implies that non-genetic factors may exert opposite influences
303 on the two DNEs.

304 Between the nine DNEs and the BAGs across nine human organ systems, we found
305 significant genetic correlations between AD1 ($g_c=0.23\pm 0.05$), ASD1 ($g_c=0.44\pm 0.05$), LLD2
306 ($g_c=0.24\pm 0.07$), SCZ1 ($g_c=0.26\pm 0.06$), and the brain BAG, and between ASD1 and the eye BAG
307 ($g_c=0.19\pm 0.07$) (**Fig. 4b** and **Supplementary eTable 4**).

308 Finally, we also found a marginally significant genetic correlation between AD2 and AD
309 ($g_c=0.22\pm 0.12$), AD1 and bipolar disorder (BIP, $g_c=-0.08\pm 0.04$), and ASD3 and BIP
310 ($g_c=0.09\pm 0.04$) using GWAS summary statistics from the psychiatric genetic consortium (**Fig. 4c**
311 and **Supplementary eTable 5**).

312 In summary, the nine DNEs demonstrate substantial genetic correlations among
313 themselves and with organ systems beyond the brain, including the eye. These findings highlight
314 the interconnectedness of the neuroanatomical patterns and genetic determinants across multiple
315 body systems and diseases, suggesting shared underlying etiological factors and potential
316 pleiotropic effects.

317

318 **The genetic colocalization of the nine DNEs**

319 To seek the shared causal variants between two clinical traits (e.g., AD1 vs. LLD2), we
320 performed Approximate Bayes Factor colocalization⁴¹ analyses (**Method 4f**) between the nine

321 DNEs (**Fig. 4d**), with the nine BAGs (**Fig. 4e**), and the six brain disorders from the psychiatric
322 genetic consortium (**Fig. 4f**).

323 Among the nine DNEs, we detected 53 causal variants (SNPs) exhibiting significant
324 colocalization signals. We showcased the shared causal variant (rs2790099 at 6p21.1) between
325 ASD2 and SCZ2 with a PP.H4.ABF=0.92. This causal SNP was mapped to the *RUNX2* gene.
326 The loss of function in *RUNX2* causes a rare autosomal dominant skeletal disorder –
327 cleidocranial dysplasia⁴², but it was implicated in ASD or SCZ in previous literature.

328 Between the nine DNEs and nine BAGs, we identified 16 causal variants (SNPs)
329 exhibiting significant colocalization signals. We showcased the shared causal variant (rs5848503
330 at 3p22.1) between ASD2 and the brain BAG with a PP.H4.ABF=0.95. One mapped gene in this
331 locus is the *MOPB* gene, which encodes the myelin-associated oligodendrocytes basic protein
332 and is actively involved in the structural constituent of the myelin sheath and nervous system
333 development. This gene was previously implicated in ASD using single-cell genomics⁴³, SCZ⁴⁴,
334 amyotrophic lateral sclerosis, and Parkinson's disease⁴⁵.

335 Between the nine DNEs and six brain diseases from the psychiatric genetic consortium,
336 we identified 7 causal variants (SNPs) exhibiting significant colocalization signals. We
337 showcased the shared causal variant (rs9257566 at 6p22.1) between ASD3 and SCZ with a
338 PP.H4.ABF=-0.82. In this locus, multiple olfactory receptor (OR) genes and the dysfunction of
339 the olfactory system were implicated in SCZ^{46,47} and ASD^{48,49}. For instance, the *OR2J2* and
340 *OR2J3* genes are two protein-coding genes in copy number variants associated with SCZ using
341 microRNA data⁵⁰. The causal SNP (rs9257566) was associated with SCZ and brain IDP, such as
342 white matter microstructural measures (**Supplementary eFigure 11**). The sensitivity checks on
343 the prior probability ($p/2$) for the three illustrations are shown in **Supplementary eFigure 12a-**
344 **c**. The causal variant, cytogenetic region, and their colocation signal direction (based on β
345 coefficients) are presented in **Supplementary eFigure 13a-c** and **Supplementary eFile 14, 15,**
346 **and 16**, respectively.

347 The genetic colocalization of the nine DNEs revealed causal genetic variants, indicating
348 that the same genomic regions may causally influence the expression of these dimensional
349 neuroimaging endophenotypes. The colocalization findings strengthen the notion that these
350 DNEs share a fundamental genetic architecture.

351

352 **The causal relationship of the nine DNEs**

353 We applied bidirectional two-sample Mendelian randomization analyses⁵¹ (**Method 4g**) to depict
354 a causal network between the nine DNEs, the eight BAGs (excluding the brain BAG), and eleven
355 chronic diseases spanning the whole-body system.

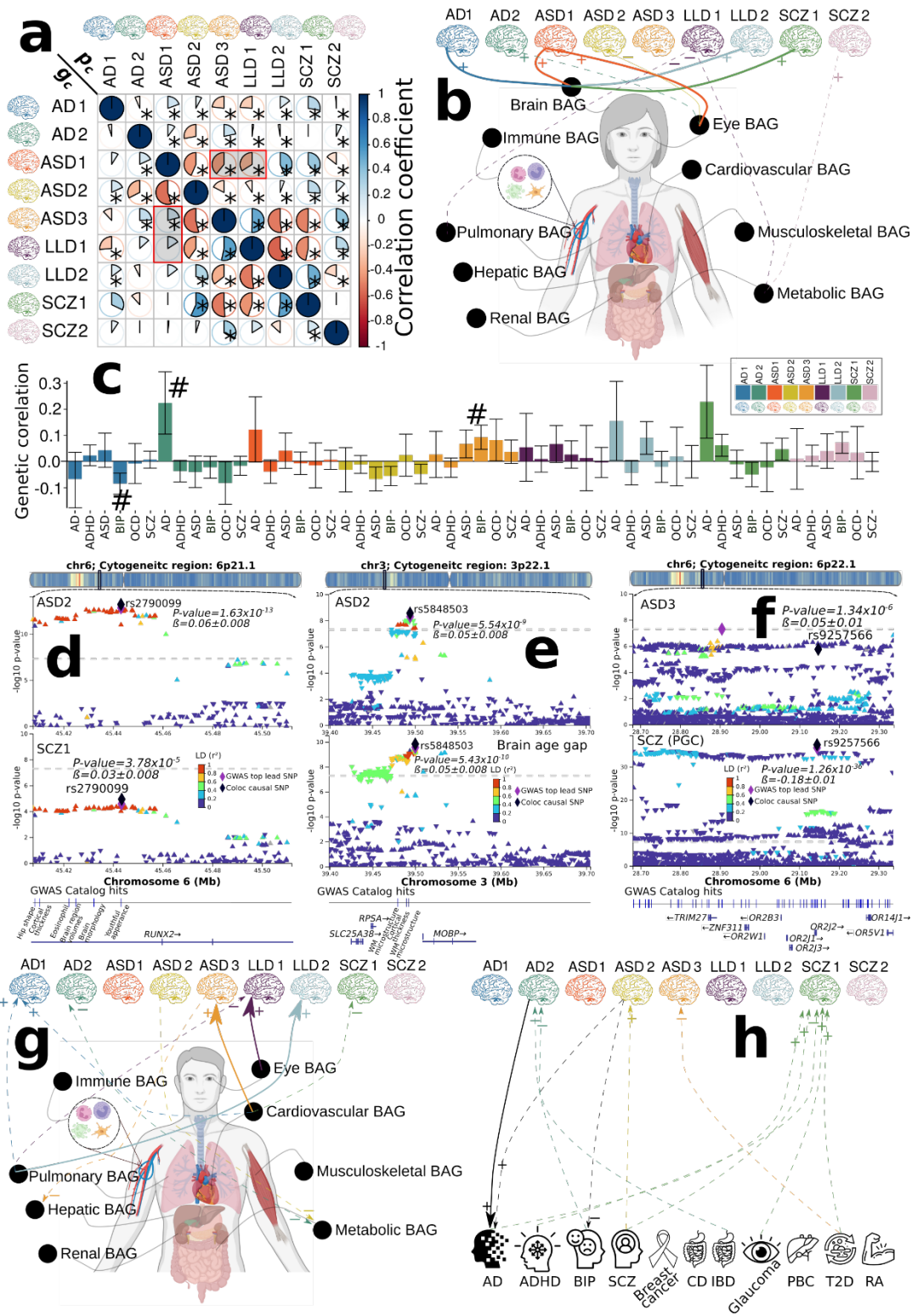
356 For each pair of DNEs, as the GWAS populations completely overlapped, conducting
357 two-sample Mendelian randomization was not feasible⁵². Alternatively, the split-sample GWAS
358 did not yield sufficient statistical power due to the limited number of instrumental variables (VI)
359 available (< 6 SNPs).

360 Among the nine DNEs and eight BAGs, we found potential causal effects of the eye
361 BAG on LLD1 [P-value=4.57x10⁻³, OR (95% CI) = 1.14 (1.04, 1.24), number of SNPs=16], the
362 cardiovascular BAG on ASD3 [P-value=6.04x10⁻³, OR (95% CI) = 1.16 (1.04, 1.29), number of
363 SNPs=34], and the pulmonary BAG on LLD2 [P-value=1.98x10⁻³, OR (95% CI) = 1.14 (1.04,
364 1.25), number of SNPs=49]. No significant causal signals persisted after the Benjamini-
365 Hochberg correction in the inverse analyses (**Fig. 4g**). Details of the results, including all five
366 different Mendelian randomization estimators, are shown in **Supplementary eFile 17**.

367 Between the nine DNEs and eleven chronic diseases, encompassing brain-related
368 conditions and diseases affecting other organs, we identified a potential causal effect from AD2
369 to AD (but not the reversed direction) using the GWAS summary statistics from the psychiatric
370 genetic consortium – the largest sample size ($N=1,126,536$) in the AD case-control study [P-
371 value= 1.74×10^{-4} , OR (95% CI) = 1.25 (1.11, 1.40), number of SNPs=7] (**Fig. 4h** and
372 **Supplementary eFigure 17**). Details of the results, including all five different Mendelian
373 randomization estimators, are shown in **Supplementary eFile 18**.

374 The Mendelian randomization results further emphasize the potential benefits of overall
375 organ health for brain-related conditions. This highlights the interconnectedness between various
376 organ systems and the brain, underscoring the significance of a holistic health and disease
377 prevention approach.

378 **Figure 4: The genetic correlation, colocalization, and causal networks of the nine DNEs**



379
 380 **a)** The genetic correlation between two DNEs (g_e , lower triangle) mirrors their phenotypic
 381 correlation (p_e , upper triangle). Red-shadowed rectangles highlight two exceptions. The symbol
 382 * indicates significant results after the Benjamini-Hochberg correction. The symbol # indicates

383 nominal significance. **b**) genetic correlations between the nine DNEs and nine biological age
384 gaps (BAG) for nine human organ systems¹⁷. Solid arrow lines (from the exposure to the
385 outcome variables) indicate significant causal relationships after the Benjamini-Hochberg
386 correction; dotted arrow lines show nominal significance (P -value <0.05). **c**) genetic correlations
387 between the nine DNEs and six neurodegenerative and neuropsychiatric disorders. **d**) genetic
388 colocalization was evidenced at one locus (6p21.1) between ASD2 and SCZ1. The signed
389 PP.H4.ABF (0.92) denotes the posterior probability (PP) of hypothesis H4, which suggests that
390 both traits share the same causal SNP (rs2790099). A positive PP indicates concordant β values
391 for both DNEs, while a negative PP implies opposite β values. **e**) genetic colocalization was
392 evidenced at one locus (3p.22.1) between ASD2 and brain BAG: PP.H4.ABF=0.95 with the
393 cause SNP rs5848503. **f**) genetic colocalization was evidenced at one locus (6p.22.1) between
394 ASD3 and SCZ case-control GWAS³⁸ from the psychiatric genetic consortium (European
395 ancestry): PP.H4.ABF=-0.82 with the cause SNP rs9257566. **g**) the causal network of the nine
396 DNEs with the eight BAGs using bidirectional Mendelian randomization. **h**) the causal network
397 of the nine DNEs with the eleven chronic diseases (e.g., AD, ADHD, BIP, and SCZ from the
398 psychiatric genetic consortium). The symbols + ($OR>1$ and $g_c>0$) and - ($OR<1$ and $g_c<0$)
399 represent a positive relationship between the two traits. Abbreviation: AD: Alzheimer's disease;
400 ADHD: Attention-deficit/hyperactivity disorder; ASD: autism spectrum disorder; BIP: bipolar
401 disorder; SCZ: schizophrenia; OCD: Obsessive-compulsive disorder; RA: rheumatoid arthritis;
402 CD: Crohn's disease; T2D: type 2 diabetes; IBD: inflammatory bowel disease; PBC: Primary
403 biliary cirrhosis.

404 405 **The nine DNEs and their PRSs significantly improve prediction for 14 systemic diseases** 406 **and mortality**

407 We investigated the added prediction power of the nine DNEs and their respective PRS (**Method**
408 **4h**) for 14 systemic diseases based on the ICD-10 code and mortality outcomes (i.e., the date of
409 death). The definition of the patient and healthy control groups and the mortality outcome are
410 presented in **Method 5**. As anticipated, the prediction performance across all tasks was modest,
411 considering that the DNEs were derived from specific disease populations. However, the DNEs
412 can significantly enhance prediction performance when combined with other commonly
413 available features (e.g., age and sex).

414 In addition to commonly available features, such as age and sex, we found that AD1,
415 ASD1, LLD1, SCZ1, and SCZ2 provided additional prediction power (i.e., incremental R^2) for
416 many disease categories (**Method 5a**). Across the 14 disease categories, the DNEs showed
417 higher incremental R^2 in mental and behavioral disorders (ICD-10 code: F) and diseases linked to
418 the central nervous system (ICD-10 code: G) than other disease categories, proving that the nine
419 DNEs in the general population capture brain disease-related effects. Combining all nine DNEs
420 further improved the incremental R^2 , especially in mental and behavioral disorders ($R^2=1.01\%$,
421 P -value= 1.74×10^{-5}) and diseases linked to the central nervous system ($R^2=0.63\%$, P -
422 value= 1.33×10^{-5}) (**Fig. 5a**). Detailed results are shown in **Supplementary eTable 6**. Results
423 using only the PRS target population are presented in **Supplementary eFigure 18**.

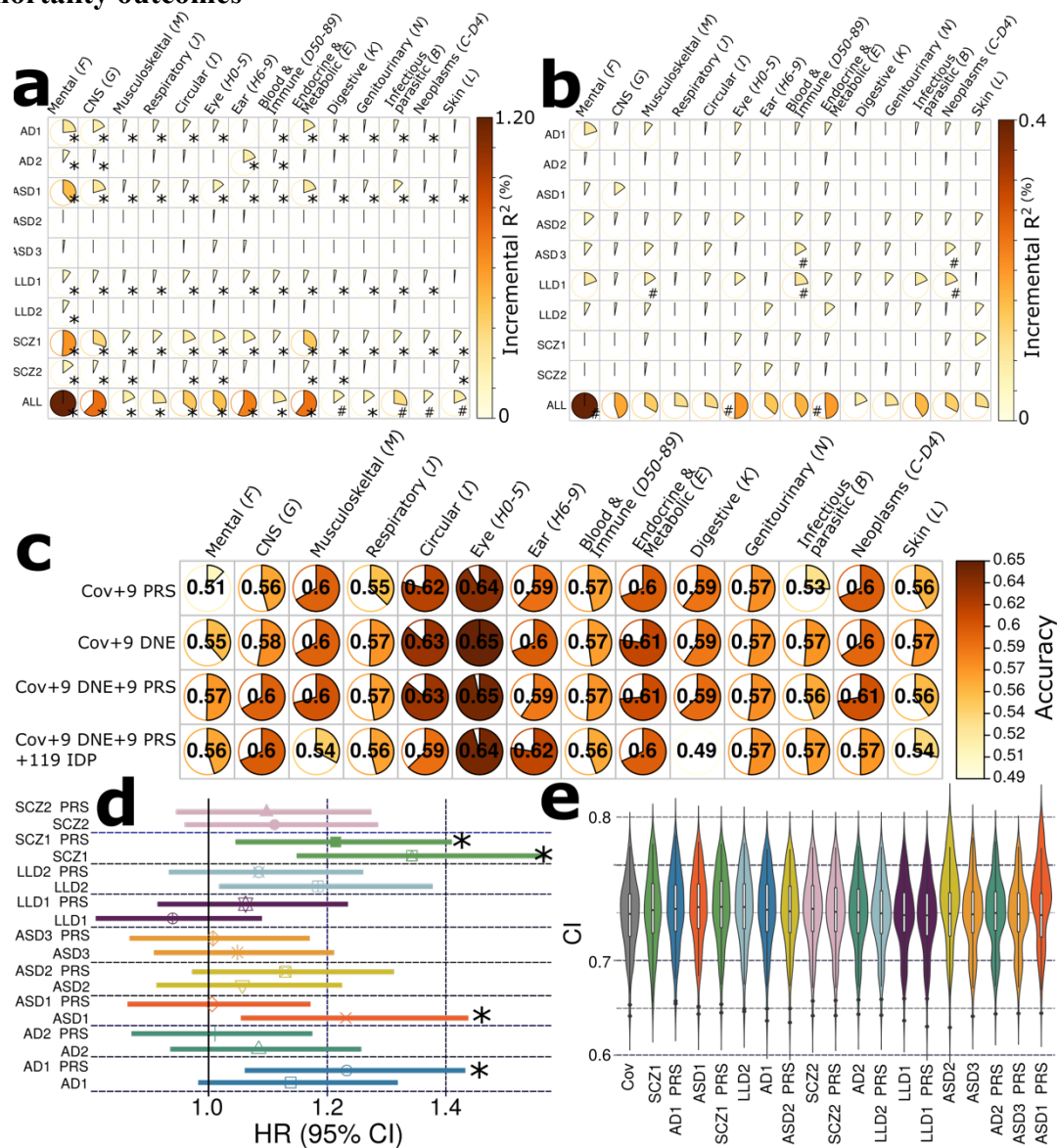
424 Compared to the nine DNEs, the nine PRSs provided smaller additional prediction power.
425 For example, the PRS for ASD3 explained an additional 0.05% of the variance (incremental R^2)
426 in diseases associated with the blood and immune systems (P -value=0.03), as well as neoplasms
427 (P -value=0.04). Combining all nine PRSs improves the incremental R^2 , particularly in mental

428 and behavioral disorders ($R^2=0.3\%$, $P\text{-value}=0.047$). No results survived the multiple
429 comparisons using the Benjamini-Hochberg method (**Fig. 5b**). Detailed results are shown in
430 **Supplementary eTable 7**.

431 We assessed the prediction ability of support vector machines (SVM) at the individual
432 level to classify the 14 disease categories (**Method 5b**). The highest performance was observed
433 for eye diseases (ICD-code: H0-5). The inclusion of PRSs, DNEs, and the combination of both,
434 along with age and sex as features, resulted in improved classification accuracy for mental and
435 behavioral disorders. For example, the accuracy increased from 0.51 to 0.55 and 0.57 for features
436 of age and sex, 9 DNEs, and 9 PRs, incrementally (**Fig. 5c**). These findings highlight the added
437 value of incorporating the nine DNEs and PRSs in predicting these disease categories. Detailed
438 results are shown in **Supplementary eTable 8**.

439 Finally, we evaluated the prediction power of the nine DNEs and PRSs for mortality risk
440 prediction using the Cox regression. Among these, SCZ1, SCZ1-PRS, ASD1, and AD1-PRS
441 were significantly associated with the risk of mortality (**Fig. 5d** and **Supplementary eTable 9a**).
442 Adding SCZ1, AD1-PRS, ASD1, and SCZ1-PRS to age and sex further improved the prediction,
443 but the performance decreased afterward (**Fig. 5e**). Lastly, incorporating the nine DNEs from the
444 second scan of 1348 participants into the model slightly increased the statistical significance and
445 the HR (**Supplementary eTable 9b** and c)

446 **Figure 5: Additional prediction power of the nine DNEs and PRSs for 14 systemic diseases**
 447 **and mortality outcomes**



448
 449 **a)** The incremental R-squared (R^2) values of the nine DNEs for predicting 14 systemic disease
 450 categories were assessed using the entire UKBB sample, with $N=39,178$ participants as
 451 independent test data. The results focusing only on the PRS target population ($N=15,891$) can be
 452 found in **Supplementary eFigure 18**. The details to derive R^2 are presented in **Method 5a**.
 453 "ALL" indicates the incremental R^2 contributed by combining the nine DNEs. **b)** The incremental
 454 R^2 of the PRS of the nine DNEs to predict 14 systemic diseases based on the ICD-10 code using
 455 only the PRS target sample. **c)** In the PRS target sample, disease classification accuracy from the
 456 independently hold-out test data ($N=5581$) was assessed using nested cross-validated support
 457 vector machines in the training/validation/test data ($N=10,000$) by fitting various sets of features
 458 (Cov indicates age and sex). **d)** The SCZ1, SCZ1-PRS, AD1-PRS, and ASD1 show significant
 459 associations with the risk of mortality in the PRS target sample. Age and sex were included as
 460 covariates in the Cox proportional hazard model. **e)** The nine DNEs and PRSs were cumulatively

461 included as features in cross-validation for mortality risk prediction. The symbol * indicates
462 significant results that survived the Benjamini-Hochberg correction. The symbol # indicates
463 nominal significance. HR: hazard ratio; CI: concordance index.

464 **Discussion**

465 This study investigated the manifestation of nine disease-related brain endophenotypes – derived
466 from four case-control studies via semi-supervised AI methods – in the general population of
467 39,178 participants in UKBB. We assessed commonalities and differences among the nine
468 DNEs, their genetic correlates in the general population, their relationships with the multiple
469 human organ systems, and their predictive capacity for 14 systemic disease categories and
470 mortality. Our findings demonstrate the clinical applicability of the nine AI-derived DNEs in
471 identifying high-risk individuals within the general population prone to developing the four
472 major brain disorders.

473 474 **Shared neuroanatomical patterns and genetic determinants across the four brain diseases** 475 **in the general population**

476 Understanding the etiology of neurodegenerative and neuropsychiatric diseases is a complex and
477 ongoing challenge in medical research^{15,16,34,36–39,53}. Our results suggest that shared underlying
478 mechanisms and genetic factors may contribute to these disorders' development and progression
479 in the general population. This notion of shared etiology across the four major neurodegenerative
480 and neuropsychiatric diseases, namely ASD, SCZ, LLD, and AD, has garnered considerable
481 attention and reshapes our understanding of these conditions^{15,16}.

482 Despite the inherent heterogeneity among neuroanatomical patterns observed in different
483 brain diseases (**Fig. 2a**), a notable commonality exists regarding their manifestations, which
484 might emanate from underlying mechanisms sharing neuropathologic characteristics and
485 pathways. As an illustration, AD1, LLD2, and SCZ1 exhibited a negative correlation (brain
486 atrophy) with global cortical volume (e.g., bilateral insula and middle frontal gyrus). This aligns
487 with expectations, considering that the UKBB population includes individuals primarily from
488 mid to late life (above 45 years), evidenced by the brain chart of the human lifespan⁵⁴. From an
489 etiological standpoint, various factors can contribute to the global cortical volume reduction
490 within the general population, with late-onset neurodegenerative and neuropsychiatric disorders
491 and aging exerting a significant impact. Likewise, ASD2 and SCZ2 exhibited a positive
492 association with the basal ganglia, including the globus pallidum. This could imply the existence
493 of potential protective genetic or environmental factors that collectively contribute to the concept
494 of "brain reserve", which might mitigate volume loss in a portion of the general population.
495 Notably, we previously revealed that individuals predominantly expressing SCZ2 exhibited
496 higher levels of education⁴ and higher rates of remission compared to the group primarily
497 influenced by SCZ1. Alternatively, these volume increases might reflect neuropathologic
498 mechanisms, such as disrupted connectivity, which are not necessarily associated with
499 neurodegenerative and neurodevelopmental components related to relatively lower brain
500 volumes.

501 Overall, the commonalities in neuroanatomical patterns across brain diseases can be
502 attributed to several factors. First, shared genetic factors may influence brain structure and
503 function^{26,55,56}, contributing to similar neuroanatomical alterations across different diseases. For
504 example, in one recent meta-analysis of 193 studies⁵⁷, the authors found a common brain
505 network defined by positive connectivity to the anterior cingulate and insula and negative
506 connectivity to the posterior parietal and lateral occipital cortex among six psychiatric disorders.
507 Genetically, this was largely evidenced by our genetic correlation (**Fig. 4a**) and colocalization
508 results (**Fig. 4d**). For instance, ASD2 showed prominent positive genetic overlap with SCZ1.

509 Historically, there has been a long-standing association between ASD and SCZ, leading to the
510 notion that autism could be a form of "childhood schizophrenia"⁵⁸. This conceptual link between
511 the two conditions has been debated and discussed. Previous case-control neuroimaging studies
512 demonstrated divergent structural and functional brain patterns in individuals with ASD
513 compared to those with SCZ⁵⁹, largely ignoring the neuroanatomical heterogeneity within each
514 condition. Genetic variants that impact key signaling pathways, synaptic function, and neuronal
515 connectivity^{60,61} could influence multiple disease phenotypes, leading to overlapping
516 neuroanatomical patterns. We performed additional MAGMA gene-set analysis⁶² to test the
517 genetic similarity between ASD2 and SCZ1. The most significant biological pathway underlying
518 ASD2 is the negative regulation of locomotion (GO 0040013, P-value= 2.27×10^{-5} , $\beta=0.22 \pm 0.02$),
519 implicated in biological processes that stop, prevent, or reduce the frequency, rate, or extent of
520 locomotion of a cell or organism. The most significant biological pathway for SCZ1 is the
521 negative regulation of neurotransmitter transport (GO 0051589, P-value= 1.41×10^{-5} ,
522 $\beta=0.22 \pm 0.02$), involved in biological processes that downregulate the directed movement of a
523 neurotransmitter into, out of, or within a cell. In particular, the latter supports the involvement of
524 dopamine and glutamate, two major neurotransmitters in the central nervous system, in
525 schizophrenia⁶³, and the gross abnormalities of serotonin and dopamine transporter bindings in
526 autism patients⁶⁴.

527 AD1 also shared genetic similarities with LLD1, both characterized by spatially extensive
528 brain atrophy and increased brain age. Previous studies found a higher prevalence of depressive
529 symptoms and LLD in individuals with AD compared to the general population⁶⁵⁻⁶⁷. The
530 relationship between AD and LLD likely involves multiple factors and may be bidirectional. On
531 the one hand, LLD may increase the risk of developing AD or accelerate the progression of
532 cognitive decline in individuals already affected by AD. On the other hand, AD-related changes
533 in the brain, such as neuroinflammation and neurochemical imbalances, may worsen depressive
534 symptoms in individuals with LLD.

535 Recognizing the shared etiology across the four brain diseases challenges traditional
536 diagnostic boundaries and underscores the importance of a broader perspective on clinical
537 presentations and underlying biological mechanisms. This understanding is important for
538 developing targeted and personalized approaches to patient care, leading to more effective
539 treatments and interventions.

540

541 **Beyond the brain**

542 Our findings strongly concur with a paradigm shift in treating brain diseases. While the
543 conventional approach has predominantly concentrated on interventions targeting the brain,
544 emerging evidence highlights the critical importance of considering the broader systemic and
545 environmental factors that influence disease onset and progression^{1,17,18,68,69}.

546 Unraveling the intricate interconnections between the brain and other organ systems is
547 crucial in broadening our understanding of brain diseases, as demonstrated by our findings and
548 other findings^{17,69}. The brain does not function in isolation but interacts with and is influenced by
549 various physiological systems throughout the body. Our results showed a close genetic
550 association and causality between the DNEs and the eye, cardiovascular, and pulmonary systems
551 (**Fig. 4b** and **g**). These findings parallel previous literature. For instance, eye-related pathological
552 changes have been revealed to mirror early signs of neurological and neuropsychiatric
553 conditions⁷⁰. The nervous and cardiovascular systems – the heart-brain axis – are intricately
554 linked, with brain regions controlling heart function via sympathetic and parasympathetic

555 pathways⁷¹. Dysfunctions in one system can affect the other's function, resulting in brain and
556 cardiovascular diseases. The immune system plays a crucial role in modulating inflammation and
557 neuroinflammation, which are implicated in many brain disorders, such as AD⁷², SCZ⁷³, and
558 depression⁷⁴. Similarly, the gut-brain axis highlights the bidirectional communication between
559 the gut microbiota and the brain, with emerging evidence linking alterations in the gut
560 microbiome to brain diseases such as Parkinson's disease⁷⁵ and depression⁷⁶. Understanding and
561 targeting these systemic interactions can modulate disease processes and improve treatment
562 outcomes.

563 Furthermore, considering environmental and lifestyle factors is essential in treating brain
564 diseases⁷⁷. Our previous work¹⁷ has shown that the BAGs of nine human organ systems comply
565 with Cheverud's Conjecture: the phenotypic correlation of two BAGs mirrors their genetic
566 correlations. However, herein we showed that the phenotypic correlation between two DNEs
567 (e.g., ASD1 vs. LLD1) did not reflect their underlying genetic correlation (**Fig. 4a**), indicating
568 potentially strong environmental and lifestyle factors that exert opposite effects on the two
569 DNEs. Furthermore, an interesting observation from our study was that the heritability estimate
570 (h^2) of early-onset diseases, such as ASD, was higher than that of late-onset diseases, such as
571 LLD, within the three neuropsychiatric disorders. This finding suggests that genetic factors play
572 a more prominent role in developing ASD at a younger age. In contrast, other factors, such as
573 environmental influences, socioeconomic factors, and lifestyle choices, may have a stronger
574 impact on developing LLD later in life. These differential heritability patterns shed light on the
575 complex interplay between genetic and non-genetic factors in the etiology of neurodegenerative
576 and neuropsychiatric disorders across different stages of life. These heritability patterns aligned
577 with a previous study that examined multiple GWAS drawn from more than 200,000 patients for
578 25 brain-associated disorders and 17 phenotypes¹⁶.

579 In conclusion, going beyond the brain is crucial for understanding and treating brain
580 diseases. By considering the connections between the brain and other organ systems,
581 understanding the impact of environmental and lifestyle factors, and harnessing the power of
582 advanced AI technologies, we can develop more effective and personalized approaches to
583 prevent, diagnose, and treat brain diseases.

584

585 **AI-derived DNEs for precision diagnostics in the general population**

586 The present study leverages cutting-edge, semi-supervised AI methods⁷⁸ and open science
587 advancements to enhance our understanding of disease heterogeneity in neurodegenerative and
588 neuropsychiatric disorders^{1-3,6,9}. In this context, implementing these AI-derived DNEs at early
589 disease or preclinical stages – in the general population – may facilitate the identification of
590 individuals at risk, and the initiation of proactive interventions before the onset of noticeable
591 symptoms, likely leading to more effective treatments and interventions and better outcomes.

592 The proposed AI-derived DNEs capture intricate brain structure and function variations,
593 often subtle and spatially complex, which traditional diagnostic methods and case-control studies
594 may overlook. By quantifying the neuroanatomical patterns associated with specific brain
595 disorders, DNEs may offer a personalized disease vulnerability assessment, inform interventions
596 at early preclinical stages, and potentially prevent or delay the onset of symptoms. At the
597 individual level, integrating genetic information (i.e., PRSs) with DNEs significantly improves
598 prediction performance for 14 systemic diseases and mortality outcomes (**Fig. 5**). In addition, our
599 Mendelian randomization analyses supported the well-established endophenotype hypothesis in
600 genetic psychiatry²¹ – endophenotype in psychiatric disorders resides inside the causal pathway

601 from underlying genetics to their exo-phenotypes (i.e., the disease itself), thereby being closer to
602 its etiology. We found that AD2, characterized by focal medial temporal lobe atrophy, exerted a
603 causal relationship with AD. However, we did not find evidence of a reverse causal relationship,
604 suggesting that the underlying genetics may influence the development of AD through the DNE,
605 although it may not be the exclusive pathway contributing to the disease. This highlights the role
606 of genetics in influencing the disease process, particularly through the identified DNE, shedding
607 light on potential pathways and mechanisms involved in AD development.

608 The present study has several limitations. Firstly, the genetic analysis focused exclusively
609 on common genetic variants. Future investigations should explore the contribution of rare
610 variants to these brain diseases. Secondly, it is important to recognize that our GWAS analyses
611 predominantly involved participants of European ancestry, limiting the generalizability of the
612 genetic findings to other populations with different ancestral backgrounds. Further research
613 efforts are necessary to collect more diverse genetic data and include underrepresented ethnic
614 groups to enhance the generalizability of the findings. Additionally, the validation of the nine
615 DNEs would benefit from additional longitudinal analyses. Fortunately, ongoing efforts to
616 collect longitudinal brain MRI data in UKBB⁷⁹ hold promise for providing valuable insights to
617 the scientific community and advancing the field of precision medicine.

618 Together, our AI-derived DNEs have emerged as novel instruments for precision
619 medicine. By capturing the complexity and heterogeneity of brain disorders, DNEs provide a
620 better understanding of disease pathology, facilitate personalized risk assessment, and hold
621 promise for targeted interventions and population selection.

622 **Methods**

623 **Method 1: Study populations**

624 Our previous studies used semi-supervised AI models to define the nine DNEs from four disease
625 case-control populations. These populations consisted of 865 healthy controls (CN), 1096
626 individuals with mild cognitive impairment (MCI), and 414 AD patients from ADNI¹⁹, 362
627 typically developing controls and 307 patients with autism spectrum disorder (ASD) from
628 ABIDE²⁰, 495 healthy controls and 501 LLD patients from the LLD study³, and 364 healthy
629 controls and 307 SCZ patients from PHENOM⁴. For more detailed information about the
630 characteristics of the study populations, please refer to the original papers.

631 The trained AI models were then applied to the UKBB general population as independent
632 data. UKBB is a population-based study of approximately 500,000 people recruited between
633 2006 and 2010 from the United Kingdom. The UKBB study has ethical approval, and the ethics
634 committee is detailed here: [https://www.ukbiobank.ac.uk/learn-more-about-uk-](https://www.ukbiobank.ac.uk/learn-more-about-uk-biobank/governance/ethics-advisory-committee)
635 [biobank/governance/ethics-advisory-committee](https://www.ukbiobank.ac.uk/learn-more-about-uk-biobank/governance/ethics-advisory-committee). The current study analyzed 39,178 multimodal
636 brain MRI data from UKBB. T1-weighted MRI data were locally processed at the University of
637 Pennsylvania; imaging-derived phenotypes (IDP) from diffusion and resting-state functional
638 MRI were downloaded from UKBB. In addition, we processed the imputed genotype data²⁴ from
639 UKBB for GWAS analyses. Last, other clinical traits were also analyzed, including phenotypes
640 related to nine human organ systems^{17,18}. The current work was performed under application
641 numbers 35148 and 60698. To unbiasedly evaluate the PRS and machine learning models, we
642 defined the following populations:

- 643 • *Disease case-control populations*: The four datasets used to train the AI models and
644 define the nine DNEs from four brain diseases.
- 645 • *Independent UKBB general population (N=39,178)*: The UKBB population in which the
646 trained AI models were applied to derive the nine DNEs.
- 647 • *PRS base/target population (split1/split2) (N=15,968)*: the UKBB population was
648 divided into two splits (split1 vs. split2) in the split-sample GWAS. To derive the PRS,
649 we used the GWAS from split1 as the base data and split2 as the target data. All disease
650 and mortality prediction tasks involving PRS used only the PRS target population
651 (N=15,968).

653 **Method 2: Semi-supervised AI methods to derive the nine DNEs**

654 The methodologies used in the current study to derive the nine DNEs belong to the semi-
655 supervised learning algorithms (**Fig. 1a**) pioneered by our group. Refer to a review for details of
656 this type of modeling⁷⁸. In particular, the current study employed the HYDRA²⁷ and Surreal-
657 GAN¹⁴ models.

658
659 **(a): HYDRA**: HYDRA leverages a widely used discriminative method, i.e., support vector
660 machines (SVM), to seek the "*l-to-k*" mapping. The novelty is that HYDRA extends multiple
661 linear SVMs to the non-linear case piecewise, thereby simultaneously serving for classification
662 and clustering. Specifically, it constructs a convex polytope by combining the hyperplane from *k*
663 linear SVMs, separating the CN group from the *k* subpopulation of the PT (patient) group.
664 Intuitively, each face of the convex polytope can be regarded to encode each subtype, capturing a
665 distinct disease effect (**Supplementary eMethod 1a**).

666
667
668
669
670
671
672
673
674
675

(b): Surreal-GAN: Surreal-GAN¹⁴ dissects underlying disease-related heterogeneity via a deep representation learning approach, instead of the discriminative SVM, under the principle of semi-supervised clustering – the "*I-to-k*" mapping. The methodological advance of this method is that Surreal-GAN models disease heterogeneity as a continuous dimensional representation, enforces monotone disease severity in each dimension, and allows the non-exclusive manifestation of all dimensions in the same participant (**Supplementary eMethod 1b**).

Method 3: Imaging analyses

676 **(a): T1-weighted MRI processing:** All images were first corrected for magnetic field intensity
677 inhomogeneity.⁸⁰ A deep learning-based skull stripping algorithm was applied to remove extra-
678 cranial material. In total, 145 IDPs were generated in gray matter (GM, 119 ROIs), white matter
679 (WM, 20 ROIs), and ventricles (6 ROIs) using a multi-atlas label fusion method.⁸¹ The ROIs
680 were fit to the four machine learning models to derive the nine DNEs. The imaging quality check
681 is detailed in **Supplementary eMethod 2**. The other IDPs derived from other MRI modalities
682 (i.e., diffusion and resting-state MRI) were downloaded from UKBB.
683

684 **(b): Neuroanatomical pattern of the nine DNEs:** We assessed the neuroanatomical patterns
685 exhibited by the nine DNEs within the general population. Since the DNEs were defined based
686 on the 119 GM ROIs obtained from T1-weighted MRI scans, we aimed to test whether these
687 patterns observed in the disease populations were manifested in the general population. To this
688 end, we used a linear regression model in which each DNE was treated as the dependent
689 variable, while the ROI, age, age-squared, sex, age x sex interaction, age-squared x sex
690 interaction, intracranial volume, brain positions in the scan, and head motion were considered
691 independent variables and covariates. We employed the Bonferroni method for multiple
692 comparisons and reported significant results accordingly.
693

694 **(c): PWAS for the nine DNEs:** We performed PWAS to associate the nine DNEs to each of the
695 611 additional phenotypes (**Supplementary eFile 1**). PWAS excluded the 119 GM ROIs utilized
696 to derive the nine DNEs to prevent any potential circular effects. Instead, the analysis
697 incorporated IDPs from other modalities, such as diffusion and resting-state functional MRI. The
698 same linear or logistic (for binary trait) regression models and multiple comparison corrections
699 were employed.

700 To check the robustness of our PWAS results, we also performed two sensitivity checks:
701 *i*) sex-stratified PWAS for males and females, and *ii*) split-sample PWAS by randomly dividing
702 the entire population into two splits (sex and age did not significantly differ).
703

Method 4: Genetic analyses

705 We used the imputed genotype data for all genetic analyses, and our quality check pipeline
706 resulted in 31,929 participants with European ancestry and 6,477,810 SNPs. First, we excluded
707 related individuals (up to 2nd-degree) from the complete UKBB sample using the KING software
708 for family relationship inference.⁸² We then removed duplicated variants from all 22 autosomal
709 chromosomes. Individuals whose genetically identified sex did not match their self-
710 acknowledged sex were removed. Other excluding criteria were: *i*) individuals with more than

711 3% of missing genotypes; ii) variants with minor allele frequency (MAF) of less than 1%; iii)
712 variants with larger than 3% missing genotyping rate; iv) variants that failed the Hardy-
713 Weinberg test at 1×10^{-10} . To adjust for population stratification,⁸³ we derived the first 40 genetic
714 principle components (PC) using the FlashPCA software⁸⁴. Details of the genetic quality check
715 protocol are described elsewhere^{3,17,17,68}.

716
717 **(a): GWAS:** For GWAS, we ran a linear regression using Plink⁸⁵ for each DNE, controlling for
718 confounders of age, age-squared, sex, age x sex interaction, age-squared x sex interaction, the
719 first 40 genetic principal components, total intracranial volume, three brain position parameters
720 in the scanner, and head motion were included, as suggested by a previous study²⁶. We adopted
721 the genome-wide P-value threshold (5×10^{-8}) and annotated independent genetic signals
722 considering linkage disequilibrium (see below).

723 To check the robustness of our GWAS results, we also performed several sensitivity
724 checks: *i*) sex-stratified GWAS for males and females, *ii*) split-sample GWAS by randomly
725 dividing the entire population into two splits (sex and age did not significantly differ), *iii*)
726 comparison of the GWAS results using the 1348 participants (i.e., 1116 European ancestry) that
727 were collected for baseline and longitudinal scans from UKBB, *iv*) non-European GWAS
728 ($N=4783$), *v*) independent GWAS on ADNI whole-genome sequencing data ($N=1555$) on AD1
729 and AD2, *vi*) concordance with six European ancestry GWAS from the psychiatric genetic
730 consortium, including AD, ADHD, ASD, BIP, OCD, and SCZ (**Supplementary eTable 2**).

731
732 **(b): SNP-based heritability:** We estimated the SNP-based heritability (h^2) using GCTA³¹ with
733 the same covariates as in GWAS.

734
735 **(c): Annotation of genomic loci:** The annotation of genomic loci and mapped genes was
736 performed via FUMA⁸⁶. For the annotation of genomic loci, FUMA first defined lead SNPs
737 (correlation $r^2 \leq 0.1$, distance < 250 kilobases) and assigned them to a genomic locus (non-
738 overlapping); the lead SNP with the lowest P-value (i.e., the top lead SNP) was used to represent
739 the genomic locus. For gene mappings, three different strategies were considered. First, positional
740 mapping assigns the SNP to its physically nearby genes (a 10 kb window by default). Second,
741 eQTL mapping annotates SNPs to genes based on eQTL associations using the GTEx v8 data⁸⁷.
742 Finally, chromatin interaction mapping annotates SNPs to genes when there is a significant
743 chromatin interaction between the disease-associated regions and nearby or distant genes⁸⁶. The
744 definition of top lead SNP, lead SNP, independent significant SNP, and candidate SNP can be
745 found in **Supplementary eMethod 3**.

746
747 **(d): Phenome-wide association queries for the identified loci in the GWAS Catalog:** We
748 queried the candidate and significant independent SNPs within each locus in the EMBL-EBI
749 GWAS Catalog (query date: 2nd June 2023, via FUMA version: v1.5.4) to determine their
750 previously identified associations with any other traits. For these associated traits, we further
751 mapped them into several high-level categories for visualization purposes.

752
753 **(e): Genetic correlation:** We used the LDSC³⁰ software to estimate the pairwise genetic
754 correlation (g_c) between each pair of DNEs, as well as between the nine DNEs and 9 BAGs of
755 multiple organ systems from our previous work¹⁷ and 6 neurodegenerative and neuropsychiatric
756 disorders from the psychiatric genetic consortium (**Supplementary eTable 2**). We used the

757 precomputed LD scores from the 1000 Genomes of European ancestry. To ensure the suitability
758 of the GWAS summary statistics, we first checked that the selected study's population was
759 European ancestry; we then guaranteed a moderate SNP-based heritability h^2 estimate. Notably,
760 LDSC corrects for sample overlap and provides an unbiased estimate of genetic correlation⁸⁸.
761 Benjamini-Hochberg procedure was performed to account for multiple comparisons.

762
763 **(f): Bayesian colocalization:** We used the R package (*coloc*) to investigate the genetic
764 colocalization signals between two traits at each genomic locus. We employed the Fully
765 Bayesian colocalization analysis using Bayes Factors (*coloc.abf*). This method examines the
766 posterior probability (PP.H4.ABF: Approximate Bayes Factor) to evaluate hypothesis $H4$, which
767 suggests the presence of a single shared causal variant associated with both traits within a
768 specific genomic locus. To determine the significance of the $H4$ hypothesis, we set a threshold of
769 $PP.H4.ABF > 0.8^{41}$. All other parameters (e.g., the prior probability of p_{12}) were set as default. We
770 also performed relevant sensitivity analyses to check the robustness of our findings.

771
772 **(g): Two-sample bidirectional Mendelian randomization:** We could not perform causal
773 inference between each pair of DNEs due to the overlapped populations and low sample sizes in
774 split-sample analyses.

775 We employed a bidirectional, two-sample Mendelian randomization using the
776 TwoSampleMR package⁵¹ to infer the causal relationships between the nine DNEs and the eight
777 BAGs across nine human organ systems (excluding the brain). The forward and inverse
778 Mendelian randomization was performed between each trait pair by switching the exposure and
779 outcome variables. We applied five different Mendelian randomization methods and reported the
780 results of inverse variance weighted (IVW) in the main text and the four others (i.e., Egger,
781 weighted median, simple mode, and weighted mode estimators) in the supplement.

782 We then performed Mendelian randomization between the nine DNEs and eleven chronic
783 diseases spanning the whole-body system. These diseases include four diseases from the
784 psychiatric genetic consortium (the ASD and OCD GWAS summary statistics did not provide
785 the allele frequency information) and seven diseases unbiasedly curated in our previous work¹⁷.
786 The included clinical traits in our Mendelian randomization are presented in **Supplementary**
787 **eTable 10**. Benjamini-Hochberg correction was performed for all tested traits.

788 We performed several sensitivity analyses. First, a heterogeneity test was performed to
789 check for violating the IV assumptions. Horizontal pleiotropy was estimated to navigate the
790 violation of the IV's exclusivity assumption⁸⁹ using a funnel plot, single-SNP Mendelian
791 randomization approaches, and Mendelian randomization Egger estimator⁹⁰. Moreover, the
792 leave-one-out analysis excluded one instrument (SNP) at a time and assessed the sensitivity of
793 the results to individual SNP.

794
795 **(h): PRS calculation for the nine DNEs:** We calculated the PRS⁹¹ using the GWAS results
796 from the split-sample analyses. The weights of the PRS were defined based on split1 data (base
797 data), and the split2 GWAS summary statistics were used as the target data for PRS calculation.
798 The QC steps for the base data are as follows: *i*) removal of duplicated and ambiguous SNPs for
799 the base data; *ii*) clumping the base GWAS data; *iii*) pruning to remove highly correlated SNPs
800 in the target data; *iv*) removal of high heterozygosity samples in the target data; *v*) removal of
801 duplicated, mismatching and ambiguous SNPs in the target data. After rigorous QC, we used
802 PLINK to generate PRS for the split2 population by adopting the classic C+T method (clumping

803 + thresholding). To determine the "best-fit" PRS, we performed a linear regression using the PRS
804 calculated at different P-value thresholds (0.001, 0.05, 0.1, 0.2, 0.3, 0.4, 0.5), controlling for age,
805 sex, intracellular volume, and the first forty genetic PCs. For each DNE-PRS, we chose the P-
806 value threshold with the highest incremental R^2 (**Supplementary eFigure 19**).
807

808 **Method 5: Disease and mortality outcome prediction.**

809 We employed logistic regression to calculate the incremental R-squared (R^2) statistics of the nine
810 DNEs and PRSs to predict 14 disease categories (**a**), support vector machines to classify the
811 healthy control participants from the disease groups (**b**), and Cox proportional hazard model to
812 predict mortality outcomes (**c**). The patients for the 14 disease categories were defined based on
813 the ICD-10 code from the UKBB website: <https://biobank.ndph.ox.ac.uk/ukb/field.cgi?id=40001>.
814 The healthy control group included participants without any ICD-10-based disease diagnoses.
815 The mortality outcome refers to the date of death:
816 <https://biobank.ndph.ox.ac.uk/ukb/field.cgi?id=40000>.
817

818 **(a): Pseudo R-squared (R^2) statistics of the logistic regression:** We built a null model by
819 including age, sex, intracranial volume, brain positions in the scan, and head motion as predictors
820 and the disease as the outcome variable. The alternative model took the disease-specific DNE or
821 PRS as one additional predictor. The incremental R^2 was calculated as the difference between the
822 pseudo R^2 of the alternative model and that of the null model, implemented by the *PseudoR2*
823 function from the *DescTools* R package (v 0.99.38). For the nine PRSs, we used the PRS target
824 sample ($N=15,891$). For the nine DNEs, we calculated the incremental R^2 using the entire UKBB
825 sample ($N=39,178$) and the PRS target sample ($N=15,891$).
826

827 **(b): Support vector machines to classify patients vs. controls:** Using the PRS target sample
828 ($N=15,891$), we used 10000 participants in a nested cross-validation (CV) procedure (i.e., CV
829 training/validation/test datasets) to select the hyperparameter C in SVM. In addition, we held out
830 5581 participants as an independent test dataset. In **Fig. 5c**, we only presented the classification
831 accuracy from the independent test dataset. The nested cross-validation (CV) procedure⁹²
832 involved an outer loop repeated 50 times, where 80% of the data was randomly selected for
833 training and 20% for testing. Within each outer loop iteration, an inner loop used 80% of the
834 training data for a 10-fold training/validation split.
835

836 **(c): Cox proportional hazard model to predict the date of death:** To evaluate the predictive
837 capacity of individual DNE and PRS for mortality risk, we employed a Cox proportional hazard
838 model while adjusting for covariates such as age and sex. The hazard ratio (HR) was calculated
839 and reported as the effect size measure that indicates the influence of each DNE or PRS on
840 mortality risk. Furthermore, we incrementally added the most predictive DNE or PRS to the Cox
841 model to determine when the model's performance reached saturation. The concordance index
842 (CI) was utilized to assess the model's performance using a 5-fold cross-validation procedure.
843 All survival analyses were conducted using the lifelines 0.25.7 Python package available online.

844 **Data Availability**

845 The GWAS summary statistics corresponding to this study are publicly available on the
846 MEDICINE knowledge portal (<https://labs.loni.usc.edu/medicine>) and the FUMA online
847 platform (<https://fuma.ctglab.nl/>).

848 **Code Availability**

849 The software and resources used in this study are all publicly available:

- 850 • MEDICINE: <https://labs.loni.usc.edu/medicine>, web portal for dissemination
- 851 • HYDRA: <https://github.com/anbai106/mlni>, DNEs for ASD1-3, LLD1-2, SCZ1-2
- 852 • Surreal-GAN: <https://github.com/zhijian-yang/SurrealGAN>, DNEs for AD1-2
- 853 • MLNI: <https://github.com/anbai106/mlni>, SVM classification
- 854 • PLINK: <https://www.cog-genomics.org/plink/>, GWAS, PRS
- 855 • FUMA: <https://fuma.ctglab.nl/>, gene mapping, genomic locus annotation
- 856 • GCTA: <https://yanglab.westlake.edu.cn/software/gcta/#Overview>, heritability estimates
- 857 • LDSC: <https://github.com/bulik/ldsc>, genetic correlation, partitioned heritability
- 858 • TwoSampleMR: <https://mrcieu.github.io/TwoSampleMR/index.html>, MR
- 859 • Coloc: <https://chr1swallace.github.io/coloc/>, Bayesian colocalization
- 860 • Lifelines: <https://lifelines.readthedocs.io/en/latest/>, Survival analyses

861 **Competing Interests**

862 None

863

864 **Authors' contributions**

865 Dr. Wen has full access to all the data in the study and takes responsibility for the integrity of the
866 data and the accuracy of the data analysis.

867 *Study concept and design:* Wen

868 *Acquisition, analysis, or interpretation of data:* Wen

869 *Drafting of the manuscript:* Wen

870 *Critical revision of the manuscript for important intellectual content:* all authors

871 *Statistical analysis:* Wen

872 **References**

- 873 1. Wen, J. *et al.* Genetic, clinical underpinnings of subtle early brain change along
874 Alzheimer's dimensions. 2022.09.16.508329 Preprint at
875 <https://doi.org/10.1101/2022.09.16.508329> (2022).
- 876 2. Hwang, G. *et al.* Assessment of Neuroanatomical Endophenotypes of Autism Spectrum
877 Disorder and Association With Characteristics of Individuals With Schizophrenia and the
878 General Population. *JAMA Psychiatry* (2023) doi:10.1001/jamapsychiatry.2023.0409.
- 879 3. Wen, J. *et al.* Characterizing Heterogeneity in Neuroimaging, Cognition, Clinical
880 Symptoms, and Genetics Among Patients With Late-Life Depression. *JAMA Psychiatry*
881 (2022) doi:10.1001/jamapsychiatry.2022.0020.
- 882 4. Chand, G. B. *et al.* Two distinct neuroanatomical subtypes of schizophrenia revealed using
883 machine learning. *Brain* **143**, 1027–1038 (2020).
- 884 5. Young, A. L. *et al.* Uncovering the heterogeneity and temporal complexity of
885 neurodegenerative diseases with Subtype and Stage Inference. *Nat Commun* **9**, 4273 (2018).
- 886 6. Yang, Z. *et al.* A deep learning framework identifies dimensional representations of
887 Alzheimer's Disease from brain structure. *Nat Commun* **12**, 7065 (2021).
- 888 7. Zhang, X. *et al.* Bayesian model reveals latent atrophy factors with dissociable cognitive
889 trajectories in Alzheimer's disease. *Proc Natl Acad Sci USA* **113**, E6535–E6544 (2016).
- 890 8. Vogel, J. W. *et al.* Four distinct trajectories of tau deposition identified in Alzheimer's
891 disease. *Nat Med* **27**, 871–881 (2021).
- 892 9. Wen, J. *et al.* Multi-scale semi-supervised clustering of brain images: Deriving disease
893 subtypes. *Med Image Anal* **75**, 102304 (2021).

- 894 10. Ferreira, D., Nordberg, A. & Westman, E. Biological subtypes of Alzheimer disease: A
895 systematic review and meta-analysis. *Neurology* **94**, 436–448 (2020).
- 896 11. Hodson, R. Precision medicine. *Nature* **537**, S49–S49 (2016).
- 897 12. Davatzikos, C. *et al.* Precision diagnostics based on machine learning-derived imaging
898 signatures. *Magnetic Resonance Imaging* **64**, 49–61 (2019).
- 899 13. Leonenko, G. *et al.* Identifying individuals with high risk of Alzheimer’s disease using
900 polygenic risk scores. *Nat Commun* **12**, 4506 (2021).
- 901 14. Yang, Z., Wen, J. & Davatzikos, C. Surreal-GAN:Semi-Supervised Representation
902 Learning via GAN for uncovering heterogeneous disease-related imaging patterns. *ICLR*
903 (2021).
- 904 15. Wingo, T. S. *et al.* Shared mechanisms across the major psychiatric and neurodegenerative
905 diseases. *Nat Commun* **13**, 4314 (2022).
- 906 16. Anttila, V. Analysis of shared heritability in common disorders of the brain. *Science* **360**,
907 eaap8757 (2018).
- 908 17. Wen, J. *et al.* The Genetic Architecture of Biological Age in Nine Human Organ Systems.
909 *medRxiv* 2023.06.08.23291168 (2023) doi:10.1101/2023.06.08.23291168.
- 910 18. Tian, Y. E. *et al.* Heterogeneous aging across multiple organ systems and prediction of
911 chronic disease and mortality. *Nat Med* 1–11 (2023) doi:10.1038/s41591-023-02296-6.
- 912 19. Petersen, R. C. *et al.* Alzheimer’s Disease Neuroimaging Initiative (ADNI): Clinical
913 characterization. *Neurology* **74**, 201–209 (2010).
- 914 20. Di Martino, A. *et al.* Enhancing studies of the connectome in autism using the autism brain
915 imaging data exchange II. *Sci Data* **4**, 170010 (2017).

- 916 21. Kendler, K. & Neale, M. Endophenotype: a conceptual analysis. *Mol Psychiatry* **15**, 789–
917 797 (2010).
- 918 22. Cannon, T. D. & Keller, M. C. Endophenotypes in the Genetic Analyses of Mental
919 Disorders. *Annual Review of Clinical Psychology* **2**, 267–290 (2006).
- 920 23. Gottesman, I. I. & Gould, T. D. The endophenotype concept in psychiatry: etymology and
921 strategic intentions. *Am J Psychiatry* **160**, 636–645 (2003).
- 922 24. Bycroft, C. *et al.* The UK Biobank resource with deep phenotyping and genomic data.
923 *Nature* **562**, 203–209 (2018).
- 924 25. Alfaro-Almagro, F. *et al.* Image processing and Quality Control for the first 10,000 brain
925 imaging datasets from UK Biobank. *Neuroimage* **166**, (2018).
- 926 26. Elliott, L. T. *et al.* Genome-wide association studies of brain imaging phenotypes in UK
927 Biobank. *Nature* **562**, 210–216 (2018).
- 928 27. Varol, E., Sotiras, A. & Davatzikos, C. HYDRA: Revealing heterogeneity of imaging and
929 genetic patterns through a multiple max-margin discriminative analysis framework.
930 *NeuroImage* **145**, 346–364 (2017).
- 931 28. Zhang, H., Schneider, T., Wheeler-Kingshott, C. A. & Alexander, D. C. NODDI: Practical
932 in vivo neurite orientation dispersion and density imaging of the human brain. *NeuroImage*
933 **61**, 1000–1016 (2012).
- 934 29. Buniello, A. *et al.* The NHGRI-EBI GWAS Catalog of published genome-wide association
935 studies, targeted arrays and summary statistics 2019. *Nucleic Acids Res* **47**, D1005–D1012
936 (2019).
- 937 30. Bulik-Sullivan, B. K. *et al.* LD Score regression distinguishes confounding from
938 polygenicity in genome-wide association studies. *Nat Genet* **47**, 291–295 (2015).

- 939 31. Yang, J., Lee, S. H., Goddard, M. E. & Visscher, P. M. GCTA: A Tool for Genome-wide
940 Complex Trait Analysis. *Am J Hum Genet* **88**, 76–82 (2011).
- 941 32. Speed, D., Holmes, J. & Balding, D. J. Evaluating and improving heritability models using
942 summary statistics. *Nat Genet* **52**, 458–462 (2020).
- 943 33. Evans, L. M. *et al.* Comparison of methods that use whole genome data to estimate the
944 heritability and genetic architecture of complex traits. *Nat Genet* **50**, 737–745 (2018).
- 945 34. Wightman, D. P. *et al.* A genome-wide association study with 1,126,563 individuals
946 identifies new risk loci for Alzheimer’s disease. *Nat Genet* **53**, 1276–1282 (2021).
- 947 35. Demontis, D. *et al.* Genome-wide analyses of ADHD identify 27 risk loci, refine the
948 genetic architecture and implicate several cognitive domains. *Nat Genet* **55**, 198–208
949 (2023).
- 950 36. Grove, J. *et al.* Identification of common genetic risk variants for autism spectrum disorder.
951 *Nat Genet* **51**, 431–444 (2019).
- 952 37. Mullins, N. *et al.* Genome-wide association study of more than 40,000 bipolar disorder
953 cases provides new insights into the underlying biology. *Nat Genet* **53**, 817–829 (2021).
- 954 38. Trubetskoy, V. *et al.* Mapping genomic loci implicates genes and synaptic biology in
955 schizophrenia. *Nature* **604**, 502–508 (2022).
- 956 39. International Obsessive Compulsive Disorder Foundation Genetics Collaborative (IOCDF-
957 GC) and OCD Collaborative Genetics Association Studies (OC GAS). Revealing the
958 complex genetic architecture of obsessive-compulsive disorder using meta-analysis. *Mol*
959 *Psychiatry* **23**, 1181–1188 (2018).
- 960 40. Cheverud, J. M. A COMPARISON OF GENETIC AND PHENOTYPIC
961 CORRELATIONS. *Evolution* **42**, 958–968 (1988).

- 962 41. Giambartolomei, C. *et al.* Bayesian Test for Colocalisation between Pairs of Genetic
963 Association Studies Using Summary Statistics. *PLOS Genetics* **10**, e1004383 (2014).
- 964 42. Hordyjewska-Kowalczyk, E. *et al.* Functional analysis of novel RUNX2 mutations
965 identified in patients with cleidocranial dysplasia. *Clin Genet* **96**, 429–438 (2019).
- 966 43. Wamsley, B. *et al.* Molecular cascades and cell-type specific signatures in ASD revealed by
967 single cell genomics. 2023.03.10.530869 Preprint at
968 <https://doi.org/10.1101/2023.03.10.530869> (2023).
- 969 44. Ayalew, M. *et al.* Convergent functional genomics of schizophrenia: from comprehensive
970 understanding to genetic risk prediction. *Mol Psychiatry* **17**, 887–905 (2012).
- 971 45. Siokas, V. *et al.* Myelin-associated oligodendrocyte basic protein rs616147 polymorphism
972 as a risk factor for Parkinson’s disease. *Acta Neurologica Scandinavica* **145**, 223–228
973 (2022).
- 974 46. Arnold, S. E. *et al.* Dysregulation of olfactory receptor neuron lineage in schizophrenia.
975 *Arch Gen Psychiatry* **58**, 829–835 (2001).
- 976 47. Turetsky, B. I., Moberg, P. J., Arnold, S. E., Doty, R. L. & Gur, R. E. Low olfactory bulb
977 volume in first-degree relatives of patients with schizophrenia. *Am J Psychiatry* **160**, 703–
978 708 (2003).
- 979 48. Almandil, N. B. *et al.* Exome-wide analysis identify multiple variations in olfactory
980 receptor genes (OR12D2 and OR5V1) associated with autism spectrum disorder in Saudi
981 females. *Frontiers in Medicine* **10**, (2023).
- 982 49. Kuo, P.-H. *et al.* Genome-Wide Association Study for Autism Spectrum Disorder in
983 Taiwanese Han Population. *PLOS ONE* **10**, e0138695 (2015).

- 984 50. Warnica, W. *et al.* Copy number variable microRNAs in schizophrenia and their
985 neurodevelopmental gene targets. *Biol Psychiatry* **77**, 158–166 (2015).
- 986 51. Hemani, G. *et al.* The MR-Base platform supports systematic causal inference across the
987 human phenome. *eLife* **7**, e34408 (2018).
- 988 52. Sanderson, E. *et al.* Mendelian randomization. *Nat Rev Methods Primers* **2**, 1–21 (2022).
- 989 53. 23andMe Research Team *et al.* Genome-wide association study of depression phenotypes
990 in UK Biobank identifies variants in excitatory synaptic pathways. *Nat Commun* **9**, 1470
991 (2018).
- 992 54. Bethlehem, R. a. I. *et al.* *Brain charts for the human lifespan*. 2021.06.08.447489
993 <https://www.biorxiv.org/content/10.1101/2021.06.08.447489v1> (2021)
994 doi:10.1101/2021.06.08.447489.
- 995 55. Wen, J. *et al.* Novel genomic loci and pathways influence patterns of structural covariance
996 in the human brain. 2022.07.20.22277727 Preprint at
997 <https://doi.org/10.1101/2022.07.20.22277727> (2022).
- 998 56. Zhao, B. *et al.* Genome-wide association analysis of 19,629 individuals identifies variants
999 influencing regional brain volumes and refines their genetic co-architecture with cognitive
1000 and mental health traits. *Nat Genet* **51**, 1637–1644 (2019).
- 1001 57. Taylor, J. J. *et al.* A transdiagnostic network for psychiatric illness derived from atrophy
1002 and lesions. *Nat Hum Behav* **7**, 420–429 (2023).
- 1003 58. Zeldovich, L. Cold parenting? Childhood schizophrenia? How the diagnosis of autism has
1004 evolved over time. *Science* doi: 10.1126/science.aau1206 (2018).
- 1005 59. Moreau, C. A. *et al.* Dissecting autism and schizophrenia through neuroimaging genomics.
1006 *Brain* **144**, 1943–1957 (2021).

- 1007 60. Berezcki, E. *et al.* Synaptic markers of cognitive decline in neurodegenerative diseases: a
1008 proteomic approach. *Brain* **141**, 582–595 (2018).
- 1009 61. Jiang, C.-C. *et al.* Signalling pathways in autism spectrum disorder: mechanisms and
1010 therapeutic implications. *Sig Transduct Target Ther* **7**, 1–36 (2022).
- 1011 62. Leeuw, C. A. de, Mooij, J. M., Heskes, T. & Posthuma, D. MAGMA: Generalized Gene-
1012 Set Analysis of GWAS Data. *PLOS Computational Biology* **11**, e1004219 (2015).
- 1013 63. McCutcheon, R. A., Krystal, J. H. & Howes, O. D. Dopamine and glutamate in
1014 schizophrenia: biology, symptoms and treatment. *World Psychiatry* **19**, 15–33 (2020).
- 1015 64. Nakamura, K. *et al.* Brain Serotonin and Dopamine Transporter Bindings in Adults With
1016 High-Functioning Autism. *Archives of General Psychiatry* **67**, 59–68 (2010).
- 1017 65. Chi, S., Yu, J.-T., Tan, M.-S. & Tan, L. Depression in Alzheimer’s disease: epidemiology,
1018 mechanisms, and management. *J Alzheimers Dis* **42**, 739–755 (2014).
- 1019 66. Dafsari, F. S. & Jessen, F. Depression—an underrecognized target for prevention of
1020 dementia in Alzheimer’s disease. *Transl Psychiatry* **10**, 1–13 (2020).
- 1021 67. Ly, M. *et al.* Late-life depression and increased risk of dementia: a longitudinal cohort
1022 study. *Transl Psychiatry* **11**, 1–10 (2021).
- 1023 68. Wen, J. *et al.* The Genetic Heterogeneity of Multimodal Human Brain Age. *bioRxiv*
1024 2023.04.13.536818 (2023) doi:10.1101/2023.04.13.536818.
- 1025 69. Zhao, B. *et al.* Heart-brain connections: Phenotypic and genetic insights from magnetic
1026 resonance images. *Science* **380**, abn6598 (2023).
- 1027 70. Woo, M. Eyes hint at hidden mental-health conditions. *Eyes hint at hidden mental-health*
1028 *conditions* <https://www.nature.com/articles/d41586-019-01114-9> (2019).

- 1029 71. Tahsili-Fahadan, P. & Geocadin, R. G. Heart–Brain Axis. *Circulation Research* **120**, 559–
1030 572 (2017).
- 1031 72. Leng, F. & Edison, P. Neuroinflammation and microglial activation in Alzheimer disease:
1032 where do we go from here? *Nat Rev Neurol* **17**, 157–172 (2021).
- 1033 73. Murphy, C. E., Walker, A. K. & Weickert, C. S. Neuroinflammation in schizophrenia: the
1034 role of nuclear factor kappa B. *Transl Psychiatry* **11**, 1–13 (2021).
- 1035 74. Miller, A. H. & Raison, C. L. The role of inflammation in depression: from evolutionary
1036 imperative to modern treatment target. *Nat Rev Immunol* **16**, 22–34 (2016).
- 1037 75. Tan, A. H., Lim, S. Y. & Lang, A. E. The microbiome–gut–brain axis in Parkinson disease
1038 — from basic research to the clinic. *Nat Rev Neurol* **18**, 476–495 (2022).
- 1039 76. Morais, L. H., Schreiber, H. L. & Mazmanian, S. K. The gut microbiota–brain axis in
1040 behaviour and brain disorders. *Nat Rev Microbiol* **19**, 241–255 (2021).
- 1041 77. Tost, H., Champagne, F. A. & Meyer-Lindenberg, A. Environmental influence in the brain,
1042 human welfare and mental health. *Nat Neurosci* **18**, 1421–1431 (2015).
- 1043 78. Wen, J. *et al.* Subtyping brain diseases from imaging data. Preprint at
1044 <https://doi.org/10.48550/arXiv.2202.10945> (2022).
- 1045 79. UKBB, U. Ambitious project announced to create the world’s largest longitudinal imaging
1046 dataset. [https://www.ukbiobank.ac.uk/learn-more-about-uk-biobank/news/ambitious-](https://www.ukbiobank.ac.uk/learn-more-about-uk-biobank/news/ambitious-project-announced-to-create-the-world-s-largest-longitudinal-imaging-dataset)
1047 [project-announced-to-create-the-world-s-largest-longitudinal-imaging-dataset](https://www.ukbiobank.ac.uk/learn-more-about-uk-biobank/news/ambitious-project-announced-to-create-the-world-s-largest-longitudinal-imaging-dataset).
- 1048 80. Tustison, N. J. *et al.* N4ITK: improved N3 bias correction. *IEEE Trans. Med. Imaging* **29**,
1049 1310–1320 (2010).

- 1050 81. Doshi, J. *et al.* MUSE: MUlti-atlas region Segmentation utilizing Ensembles of registration
1051 algorithms and parameters, and locally optimal atlas selection. *Neuroimage* **127**, 186–195
1052 (2016).
- 1053 82. Manichaikul, A. *et al.* Robust relationship inference in genome-wide association studies.
1054 *Bioinformatics* **26**, 2867–2873 (2010).
- 1055 83. Price, A. L., Zaitlen, N. A., Reich, D. & Patterson, N. New approaches to population
1056 stratification in genome-wide association studies. *Nat Rev Genet* **11**, 459–463 (2010).
- 1057 84. Abraham, G., Qiu, Y. & Inouye, M. FlashPCA2: principal component analysis of Biobank-
1058 scale genotype datasets. *Bioinformatics* **33**, 2776–2778 (2017).
- 1059 85. Purcell, S. *et al.* PLINK: A Tool Set for Whole-Genome Association and Population-Based
1060 Linkage Analyses. *Am J Hum Genet* **81**, 559–575 (2007).
- 1061 86. Watanabe, K., Taskesen, E., van Bochoven, A. & Posthuma, D. Functional mapping and
1062 annotation of genetic associations with FUMA. *Nat Commun* **8**, 1826 (2017).
- 1063 87. The GTEx Consortium. The Genotype-Tissue Expression (GTEx) project. *Nat Genet* **45**,
1064 580–585 (2013).
- 1065 88. Bulik-Sullivan, B. *et al.* An atlas of genetic correlations across human diseases and traits.
1066 *Nat Genet* **47**, 1236–1241 (2015).
- 1067 89. Bowden, J. *et al.* A framework for the investigation of pleiotropy in two-sample summary
1068 data Mendelian randomization. *Stat Med* **36**, 1783–1802 (2017).
- 1069 90. Bowden, J., Davey Smith, G. & Burgess, S. Mendelian randomization with invalid
1070 instruments: effect estimation and bias detection through Egger regression. *Int J Epidemiol*
1071 **44**, 512–525 (2015).

- 1072 91. Choi, S. W., Mak, T. S.-H. & O'Reilly, P. F. Tutorial: a guide to performing polygenic risk
1073 score analyses. *Nat Protoc* **15**, 2759–2772 (2020).
- 1074 92. Wen, J. *et al.* Convolutional neural networks for classification of Alzheimer's disease:
1075 Overview and reproducible evaluation. *Medical Image Analysis* **63**, 101694 (2020).
- 1076
- 1077

1078 **Acknowledgments**

1079 We want to express our sincere gratitude to the UK Biobank team for their invaluable
1080 contribution to advancing clinical research in our field. We extend our gratitude to the
1081 psychiatric genetic consortium (PGC: <https://pgc.unc.edu/>) for their generosity in sharing the
1082 GWAS summary statistics with the broader scientific community. This study used the UK
1083 Biobank resource under Application Numbers: 35148 and 60698. Additionally, we extend our
1084 appreciation to the psychiatric genetic consortium for their valuable contribution to sharing the
1085 GWAS summary statistics with the scientific community. Lastly, we acknowledge the
1086 collaboration between the University of Southern California, the University of Pennsylvania, and
1087 the University of Melbourne in conducting this research. We gratefully acknowledge the support
1088 of the iSTAGING consortium, funded by the National Institute on Aging through grant RF1
1089 AG054409 at the University of Pennsylvania (CD). We also acknowledge the funding provided
1090 by the National Institute of Biomedical Imaging and Bioengineering at the University of
1091 Southern California through grant 5P41EB015922-25 (AT). Additionally, we acknowledge the
1092 funding program from the Rebecca L. Cooper Foundation at the University of Melbourne (AZ).